"A Statistical Analysis of Some Non-Linear Optical Effects"

FINAL REPORT

August 20, 1971

NASA GRANT

NGR 22-017-019

Worcester Polytechnic Institute

Principal Investigator:

E. L. O'Neill, Department of Physics

Participants:

L. Estes, Department of Electrical Engineering

L. Narducci, Department of Physics

W. Clark, Department of Physics

INTRODUCTION

This Final Report contains the results of our research activities supported by NASA Grant NGR 22-017-019.

Part I deals with the scattering of light from a rotating ground glass reproduced from Dr. Richard Tuft's Ph.D. thesis.

Part II concerns itself with the counting statistics of second harmonic light generated by a pseudo-thermal source and is in the form of a reprint submitted for publication to the Journal of the Optical Society of America.

Part III describes an important theorem in Applied Optics dealing with the upper bound of the optical transfer function. In addition we have taken the liberty of enclosing reprints from a recent JOAS article dealing with some research carried out during the previous NASA grant.

PART I

Scattering of Laser Light From a Rotating Ground Glass

ABSTRACT

Experimental results concerning the statistical properties of a light beam scattered by two rotating ground glasses have been obtained. Photocount statistics measured at different scattering angles and different translational speeds of the ground glass have confirmed the known result that the scattered light amplitude is a stochastic Gaussian variable in the case that there are many scatterers in the illuminated region. Further results indicate that, as the size of the inhomogeneities on the ground glass becomes comparable to the size of the illuminated region, the field amplitude probability distribution tends toward log-amplitude normal.

Self-beating measurements on the scattered light of a He-Ne laser in a TEM_{oo} configuration have shown that the power spectrum is a Gaussian function of the frequency. The dependence of its half-width on the translational speed of the ground glass and on the focal length of the lens that focuses the beam on the scattering surface has been measured. The experimental results agree very closely with the theoretical predictions.

ACKNOWLEDGEMENTS

I wish to express my appreciation for the guidance given me by my advisor, Dr. Lorenzo M. Narducci, and by Dr. Lee E. Estes. Their enthusiasm and interest in this work provided a prime motivating factor for its successful conclusion.

Thanks are also due to Dr. Edward L. O'Neill for helpful discussions, and to Dr. John D. Kuppenheimer, whose experimental expertise was instrumental in the successful construction of the photocount system.

During the course of this work, I was supported by a NDEA Title IV Fellowship.

TABLE OF CONTENTS

LIST OF TABLES

LIST OF FIGURES

LIST OF FIGURES (CONTINUED)

Figure

STATISTICAL PROPERTIES OF LIGHT SCATTERED FROM A ROTATING GROUND GLASS

by

Richard A. Tuft

I. INTRODUCTION

When a beam of light impinges on a scatterer of linear dimensions ℓ, a diffraction pattern originates with an angular aperture $\alpha = \lambda/\ell$. If a collection of independent scatterers is placed in the path of a coherent beam of finite diameter d, the diffraction lobes will interfere with one another generating a far field pattern which is a random distribution of bright and dark areas of irregular shapes and sizes. Each bright area is known to subtend an angle of the order of λ/d which only depends on the wavelength of the incident light and the diameter d of the beam. This is also known in diffraction theory to be the pattern generated by a collection of holes randomly distributed over an opaque screen.[1] If the scatterers are set in motion, the diffraction pattern exhibits local fluctuations of intensity.

Although the distribution function of the scattered electric field amplitude is expected to be Gaussian[2] regardless of the details of the motion of the scattering medium, if the phases of the diffracted lobes are random and if a large enough number of independent scatterers are illuminated, the field intensity correlation function does depend on the type of motion the scatterers are undergoing. For example, if a large enough number of scatterers are undergoing Brownian motion, it has been proved that the spectrum $I(\omega)$ of the scattered light is Lorentzian.[3]

An interesting situation arises when a beam of light is scattered by a piece of ground glass which is set in motion, for example, with constant angular velocity. It is reasonable to assume that different microareas of the ground glass scatter independently of one another. However, the motion of the scatterers through the illuminated area is characterized by a velocity distribution which is a delta function centered at the value of the velocity of translation.[4] In a certain sense particles in Brownian motion and the microareas of a ground glass represent extreme cases in which the motion of the scatterers is, respectively, completely uncorrelated and fully correlated. The study of the field scattered by a rotating ground glass

appears to have some bearing, therefore, on the much more complicated problem of the light scattering from density fluctuations in a medium where a finite correlation exists between different coherence volumes.[5]

We are presently interested in studying the statistical properties of a coherent light beam scattered by a rotating ground glass for a variety of surfaces characterized by different average irregularities. We discuss results for two ground glasses with average irregularities on the order of one micron and 20 microns respectively.

In Chapter II we treat the problem of the power density spectrum of the scattered light. The calculations and the experimental verifications of the theory are presented.

In Chapter III we briefly touch upon the formalism of photocount statistics and then describe the construction of a photocount experiment and the experimental results.

II. THE POWER SPECTRUM OF THE SCATTERED LIGHT

A. Theoretical Description of the Spectral Broadening

In this section we derive a theoretical expression for the power density spectrum of the scattered light. We will consider the problem in the scalar approximation, thus ignoring depolarization phenomena.

We will first consider the formation of the laser spot on the ground glass. With reference to Figure 1, the laser beam B is incident from the left upon the lens, which is located in the (u,v) plane. Since the laser is a Spectra Physics model 119 He - Ne 6328A^{o} laser operating in a TEM_{oo} mode, the field intensity may be taken as a plane wave with a Gaussian cross-section:

$$I(x,y) = I_o \, e^{-\frac{(x^2+y^2)}{2\sigma^2}} \quad . \qquad \text{(II.1)}$$

Here σ is the "radius" of the incident beam, and in this case is known to be on the order of 0.5 mm.[6] We now consider the lens to be aberration free, so that it merely superimposes a quadratic phase factor upon the incident beam. Thus, at the exit pupil of the lens, we have an electric field amplitude of the form

$$E(u,v) = E_o \exp\left\{-\left(\frac{1}{4\sigma^2} + \frac{ik}{2f}\right)(u^2+v^2)\right\} . \qquad \text{(II.2)}$$

Figure 1

Formation of laser spot on ground glass.

B, incident laser beam; 1, (u,v) plane of lens;

f, focal length of lens;

z, distance between lens and ground glass;

2, (x_1,y_1) plane of ground glass;

P, laser beam propagation axis.

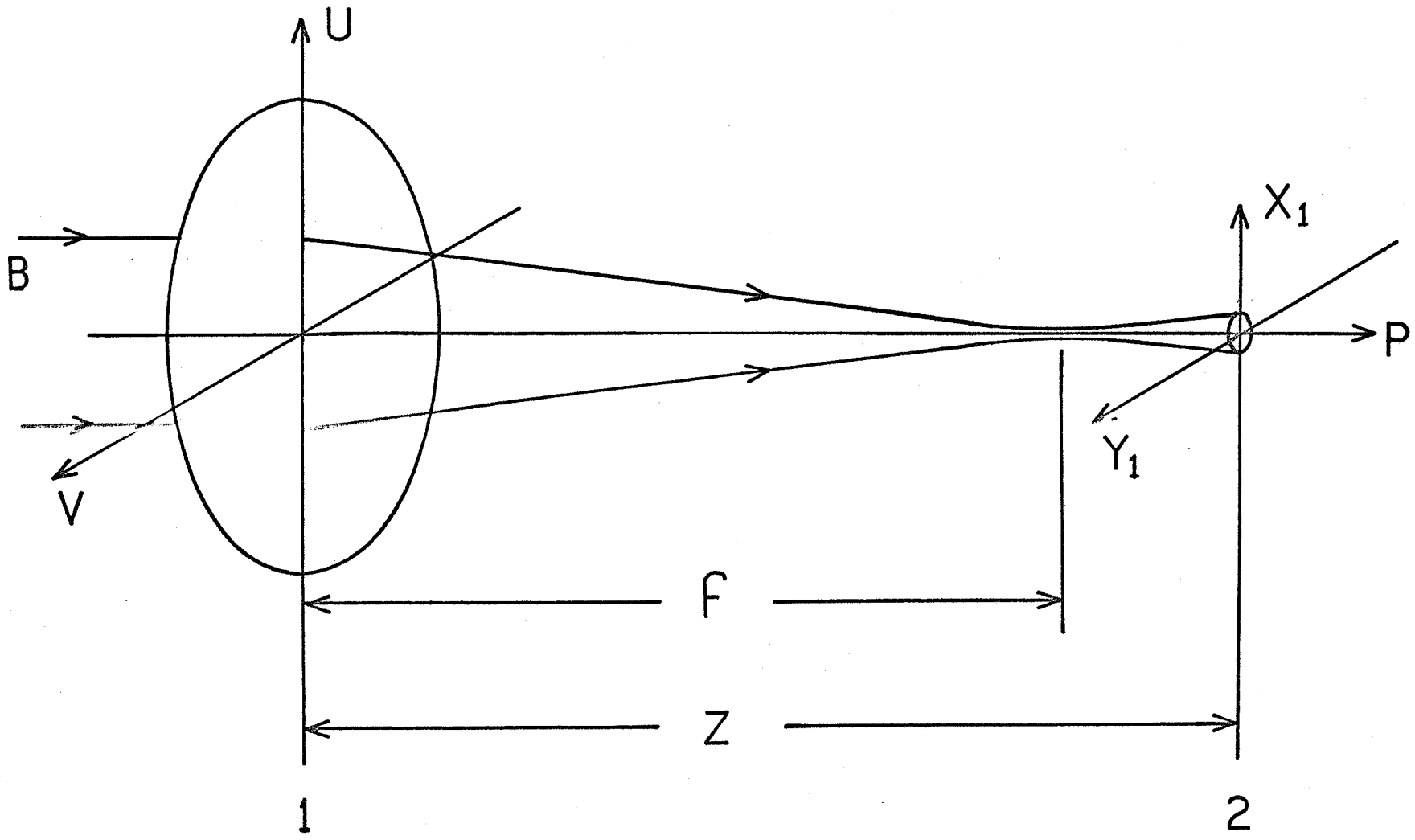
U
B
V
X1
Y1
P
f
Z
1
2

To obtain the electric field amplitude in the (x_1, y_1) plane of the ground glass, we propagate the field of Eq. II.2 a distance z by means of the Fresnel diffraction formula[7]

$$E(x_1, y_1) = \frac{-ike^{ikz}}{2\pi z} \iint du\,dv\; E(u,v) \exp\left\{\frac{ik}{2z}\left[(x_1-u)^2+(y_1-v)^2\right]\right\} \quad . \tag{II.3}$$

Using the explicit form of $E(\mu,\nu)$, we obtain

$$E(x_1, y_1) = -\frac{ike^{ikz}}{2\pi z} E_0 \iint du\,dv\; \exp\left\{\frac{ik}{2z}\left[(x_1-u)^2+(y_1-v)^2\right]\right\} \cdot \tag{II.4}$$

$$\cdot \exp\left\{-\left(\frac{ik}{2f}+\frac{1}{4\sigma^2}\right)(u^2+v^2)\right\} \quad .$$

This integral is of the form:[8]

$$\int_{-\infty}^{\infty} e^{a(x_1-u)^2} e^{b(x_2-u)^2} du = \sqrt{\frac{-\pi}{a+b}}\; \exp\left[\frac{ab}{a+b}(x_1-x_2)^2\right] \quad . \tag{II.5}$$

In our case:

$$a = \frac{ik}{2z} \quad , \quad b = -\frac{1}{4\sigma^2} - \frac{ik}{2f}$$

$$x_1 = x_1 \quad , \quad x_2 = 0$$

and the integral is repeated for v. Thus

$$E(x_1, y_1) = E_0' \exp\left\{-\frac{\left(\frac{k^2}{f}-\frac{ik}{2\sigma^2}\right)(x_1^2+y_1^2)}{4z\left[\frac{1}{4\sigma^2}+\frac{ik}{2}\left(\frac{1}{f}-\frac{1}{z}\right)\right]}\right\} \tag{II.6}$$

where

$$E_0' = -\frac{ik}{2z}\; \frac{E_0\, e^{ikz}}{\frac{1}{4\sigma^2}+\frac{ik}{2}\left(\frac{1}{f}-\frac{1}{z}\right)} \quad . \tag{II.7}$$

We now look for the form which the scattered electric field amplitude assumes at the detection point, which is a distance $\vec{r}$ away from the (x_1, y_1) coordinate system. (See Figure 2) We look upon the ground glass as a collection of independent microareas of average linear dimension ℓ ,[9] located at distances $\vec{R}_j$ away from the z axis of propagation in the (x_1, y_1) plane. The microarea about the point $\vec{R}_j$ will produce an electric field at the detection point which takes the approximate form

$$E_j(\vec{r}, t) = E(\vec{R}_j(t))\, S_j \exp\left\{ i(\varphi_j + k|\vec{r} - \vec{R}_j| - \omega_0 t)\right\} \qquad \text{(II.8)}$$

where φ_j is the phase of the elementary wave at $\vec{R}_j(t)$, S_j is a shape factor which accounts for the diffraction produced by the microarea around $\vec{R}_j(t)$, and ω_0 is the angular frequency of the incident field, which has been suppressed in calculations up to this point.

We now make the expansion

$$|\vec{r} - \vec{R}_j| = \sqrt{r^2 + R_j^2 - 2\vec{r}\cdot\vec{R}_j} = r\sqrt{1 + \frac{R_j^2}{r^2} - 2\frac{\hat{n}\cdot\vec{R}_j}{r}} \qquad \text{(II.9)}$$

where $\hat{n}$ is a unit vector directed along $\vec{r}$.

thus

$$|\vec{r} - \vec{R}_j| = r\left(1 - \frac{\hat{n}\cdot\vec{R}_j}{r} + \frac{1}{2}\frac{R_j^2}{r^2} + \cdots\right) . \qquad \text{(II.10)}$$

Figure 2

Experimental setup.

(x_1,y_1), plane of ground glass; $\vec{R}_j$, radius vector to jth microarea of ground glass; $\vec{r}$, radius vector from center of laser spot to detector;

P, laser beam propagation axis;

ψ, angle between P and $\vec{r}$.

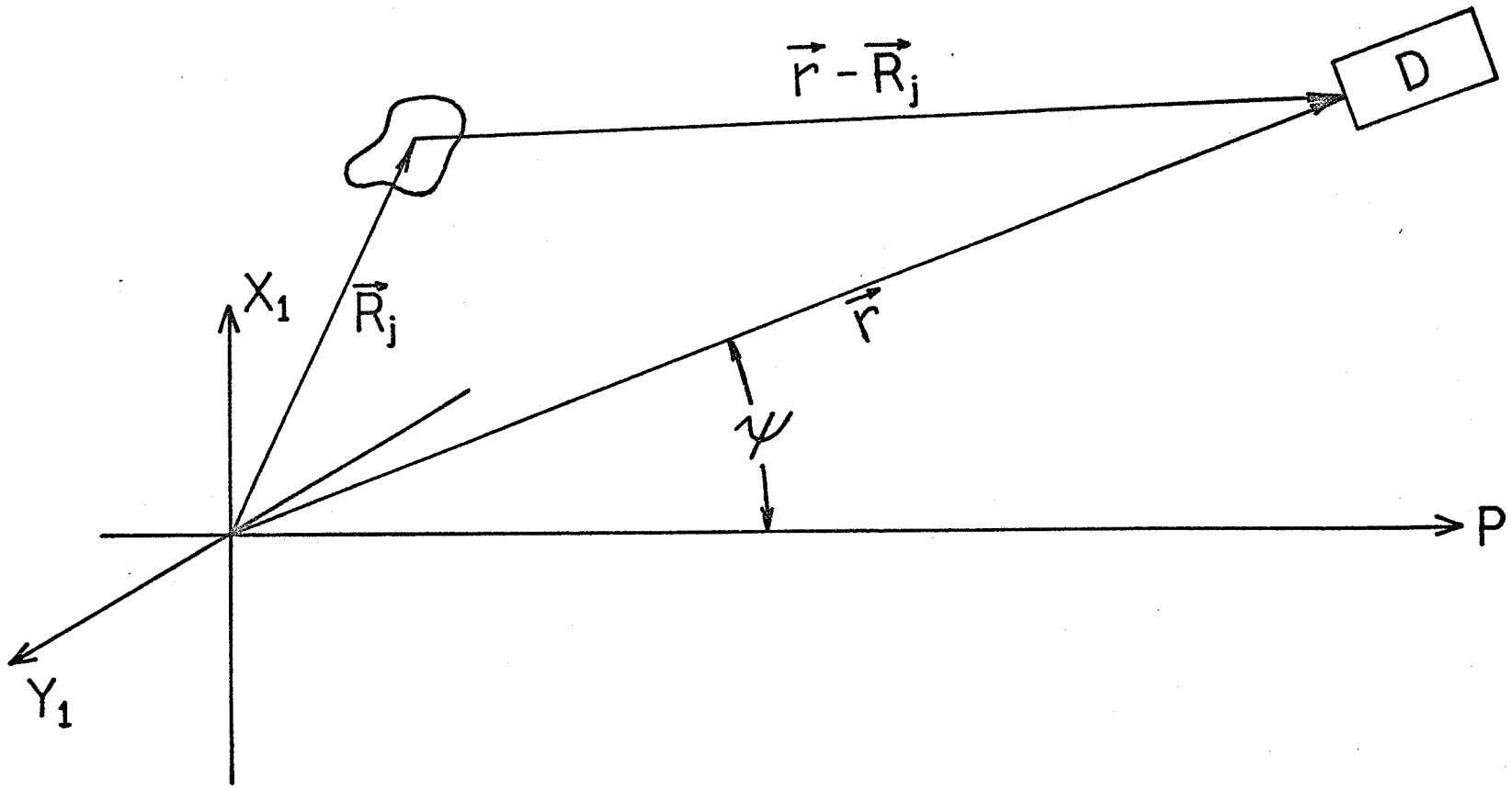
$\vec{r} - \vec{R}_j$
D
X_1
$\vec{R}_j$
$\vec{r}$
ψ
P
Y_1

Now if $|\vec{R}_j| << r$, we can neglect all terms but the first two, so

$$|\vec{r} - \vec{R}_j| \approx r - \hat{n} \cdot \vec{R}_j$$

and

$$E_j(\vec{r},t) = E(\vec{R}_j(t))\, S_j \exp\left\{i(\varphi_j + kr - \omega_0 t - k\hat{n}\cdot\vec{R}_j(t))\right\} . \quad \text{(II.11)}$$

The total field seen by the detector is the result of the coherent superposition of the elementary contributions $E_j(\vec{r},t)$:

$$\begin{aligned} E(\vec{r},t) &= \sum_j E_j(\vec{r},t) \\ &= \exp\left[i(kr-\omega_0 t)\right] \sum_j S_j\, e^{i\varphi_j} \cdot \\ &\cdot \int d^2\vec{r}_1\, E(\vec{r}_1)\, e^{-ik\hat{n}\cdot\vec{r}_1}\, \delta^{(2)}(\vec{r}_1 - \vec{R}_j(t)) , \end{aligned} \quad \text{(II.12)}$$

where $d^2\vec{r}_1 = dx_1\, dy_1$ and the integral extends over the illuminated area.

The field amplitude correlation function at the detection point is given by an average of $E(\vec{r},t)\,E^*(\vec{r},t+\tau)$ over the ensemble of phases φ_j , diffraction factors S_j , and locations of the microareas $\vec{R}_j$. Thus we have

$$\begin{aligned} \langle E(\vec{r},t)\,E^*(\vec{r},t+\tau)\rangle_{\varphi_j, S_j, \vec{R}_j} &= e^{i\omega_0\tau} \Big\langle \sum_{j\ell} S_j S_\ell\, e^{i(\varphi_j - \varphi_\ell)} \cdot \\ &\cdot \iint d^2\vec{r}_1\, d^2\vec{r}_2\, E(\vec{r}_1)E^*(\vec{r}_2)\, e^{-ik\hat{n}\cdot(\vec{r}_1-\vec{r}_2)}\, \delta^{(2)}(\vec{r}_1 - \vec{R}_j(t))\, \delta^{(2)}(\vec{r}_2 - \vec{R}_\ell(t+\tau)) \Big\rangle . \end{aligned} \quad \text{(II.13)}$$

We now assume that φ_j, s_j, and $\vec{R}_j$ are all independent random variables, so that the average factorizes. We then make use of the fact that

$$\langle e^{i(\varphi_j - \varphi_e)} \rangle = \delta_{ij} \tag{II.14}$$

to obtain

$$\langle E(\vec{r},t)E^*(\vec{r},t+\tau)\rangle = e^{i\omega_0\tau}\langle s^2\rangle \cdot$$
$$\cdot \iint d^2\vec{r}_1\, d^2\vec{r}_2\; E(\vec{r}_1)E^*(\vec{r}_2)\; e^{-ik\vec{n}\cdot(\vec{r}_1-\vec{r}_2)} G(\vec{r}_1,\vec{r}_2)\,, \tag{II.15}$$

where we have defined the density correlation function $G(\vec{r}_1,\vec{r}_2)$ as

$$G(\vec{r}_1,\vec{r}_2) = \sum_j \langle \delta^{(2)}(\vec{r}_1 - \vec{R}_j(t))\; \delta^{(2)}(\vec{r}_2 - \vec{R}_j(t+\tau))\rangle_{\vec{R}_j}\,. \tag{II.16}$$

Equation II.15 differs from a previously published result[10] in that the density correlation function weights the product of two field amplitudes rather than a field intensity.

We now use the knowledge that the ground glass is in uniform motion to construct an explicit value of $G(\vec{r}_1,\vec{r}_2)$. Since we have

$$\vec{R}_j(t) = \vec{R}_j(0) + \vec{v}\,t\,,$$

we may expand the delta functions in integral form to obtain

$$G(\vec{r}_1,\vec{r}_2) = \sum_j \iint_{-\infty}^{\infty} \frac{d^2\vec{q}_1\, d^2\vec{q}_2}{(2\pi)^4} \exp\left\{ i\,\vec{q}_1\cdot(\vec{r}_1 - \vec{v}t) + i\,\vec{q}_2\cdot(\vec{r}_2 - \vec{v}(t+\tau))\right\}\cdot$$

$$\cdot \left\langle \exp\left\{ -i(\vec{q}_1+\vec{q}_2)\cdot\vec{R}_j(0)\right\}\right\rangle \quad . \tag{II.17}$$

If we assume that the microareas are uniformly distributed over the illuminated area A, we can write

$$\left\langle \exp\left\{ -i(\vec{q}_1+\vec{q}_2)\cdot\vec{R}_j(0)\right\}\right\rangle = \iint_{-L/2}^{L/2} \frac{dR_{jx}\, dR_{jy}}{L^2}\, e^{-i(\vec{q}_1+\vec{q}_2)\cdot\vec{R}_j(0)} \tag{II.18}$$

or

$$\left\langle e^{-i(\vec{q}_1+\vec{q}_2)\cdot\vec{R}_j(0)}\right\rangle = \operatorname{sinc}\left\{\frac{(q_1+q_2)_x L}{2}\right\} \operatorname{sinc}\left\{\frac{(q_1+q_2)_y L}{2}\right\} \tag{II.19}$$

where we have assumed a square illumination area for convenience in calculation. In the limit that L is large,[11]

$$\operatorname{sinc}\left\{\frac{(q_1+q_2)_x L}{2}\right\} \operatorname{sinc}\left\{\frac{(q_1+q_2)_y L}{2}\right\} \simeq \frac{(2\pi)^2}{L^2}\,\delta^{(2)}(\vec{q}_1+\vec{q}_2). \tag{II.20}$$

Using Eq. II.20 in Eq. II.17, and letting $L^2 = A$, the illuminated area, we have

$$G(\vec{r}_1,\vec{r}_2) = \sum_j \frac{1}{A} \int_{-\infty}^{\infty} \frac{d^2\vec{q}_1}{(2\pi)^2} \exp\left\{ i\,\vec{q}_1\cdot(\vec{r}_1 - \vec{v}t - \vec{r}_2 + \vec{v}t + \vec{v}\tau)\right\}$$

$$= \frac{N}{A}\,\delta^{(2)}(\vec{r}_1 - \vec{r}_2 + \vec{v}\tau) \tag{II.21}$$

where N is the number of scatterers in the beam. Using this expression for the density correlation function, the field correlation function, Eq. II.15, becomes

$$\langle E(\vec{r},t)E^*(\vec{r},t+\tau)\rangle = \frac{N\langle s^2\rangle}{A} \exp\{i(\omega_0 + k\hat{n}\cdot\vec{v})\tau\}\cdot \int d^2\vec{r}_1\, E(\vec{r}_1)\, E^*(\vec{r}_1 + \vec{v}\tau) \tag{II.22}$$

where $E(\vec{r}_1)$ is the incident field on the ground glass given by Eq. II.6. The frequency shift $k\hat{n}\cdot\vec{v}$ appearing in the exponent of Eq. II.22 is a Doppler shift which is zero if the direction of observation is maintained perpendicular to the direction of the velocity of translation.

The integral in Eq. II.22 can be written in the form

$$|E_0'|^2 \iint dx_1\, dy_1\; e^{a(x_1^2+y_1^2)}\; e^{a^*[(x_1+v\tau)^2 + y_1^2]} \tag{II.23}$$

where we have chosen the (x_1, y_1) axes such that $\vec{v} = (v,0,0)$. Here

$$a = \frac{-\left(\frac{k^2}{f} - \frac{ik}{2\sigma^2}\right)}{4z\left[\frac{1}{4\sigma^2} + \frac{ik}{2}\left(\frac{1}{f} - \frac{1}{z}\right)\right]} \cdot \tag{II.24}$$

Now the integral of Eq. II.23 is in the form of Eq. II.5, with $b = a^*$ Thus we have

$$\int d^2\vec{r}_1 \; E(\vec{r}_1)\, E^*(\vec{r}_1 + \vec{v}\tau)$$

$$= \frac{\pi}{2 Re\, a} \exp\left\{ \frac{-|a|^2}{2 Re\, a} v^2 \tau^2 \right\} . \qquad \text{(II.25)}$$

With this result the final form of the field amplitude correlation function, neglecting the Doppler shift, can be expressed as

$$\langle E(\vec{r},t)\, E^*(\vec{r},t+\tau) \rangle =$$

$$\frac{2\pi\sigma^2}{A} N \langle s^2 \rangle E_o^2 \, e^{i\omega_o \tau} \, e^{-\frac{v^2\tau^2}{2}\left(\frac{k^2\sigma^2}{f^2} + \frac{1}{4\sigma^2}\right)} . \qquad \text{(II.26)}$$

The field power spectrum $I(\omega)$, according to the Wiener-Khintchine theorem,[12] is the time Fourier transform of Eq. II.26;

$$I(\omega) = \frac{1}{\sqrt{2\pi}} \int_{-\infty}^{\infty} d\tau \; e^{-i\omega\tau} \langle E(\vec{r},t)\, E^*(\vec{r},t+\tau) \rangle$$

$$= \frac{2\pi\sigma^2}{A} \frac{N \langle s^2 \rangle E_o^2}{\left[v^2 \left(\frac{k^2\sigma^2}{f^2} + \frac{1}{4\sigma^2} \right) \right]^{1/2}} \; e^{-\frac{(\omega - \omega_o)^2}{2v^2\left(\frac{k^2\sigma^2}{f^2} + \frac{1}{4\sigma^2}\right)}} . \qquad \text{(II.27)}$$

$I(\omega)$ is a Gaussian function of frequency centered around the angular frequency ω_o of the incident field. The half-width at half-height of $I(\omega)$ is

$$\Delta\omega_{1/2} = (2\ln 2)^{1/2} v \left(\frac{k^2\sigma^2}{f^2} + \frac{1}{4\sigma^2} \right)^{1/2}. \qquad \text{(II.28)}$$

There are several features of $\Delta\omega_{1/2}$ worth noting. First of all, as one might expect, the power spectrum broadening is directly proportional to the translational velocity of the microareas across the illuminated region. Secondly, for focal lengths $f \gtrsim 5\,cm$, the $\frac{1}{4\sigma^2}$ term is negligible, resulting in a power spectrum broadening which is inversely proportional to the focal length of the focusing objective and linearly related to the dimensions of the incident beam.

It is interesting to note that the power spectrum broadening $\Delta\omega_{1/2}$ is predicted to be independent of the parameter z. Equation II.28, in fact, indicates that no matter how far out of focus one sets the surface of the ground glass, the half width $\Delta\omega_{1/2}$ remains constant, every other parameter being fixed.

We have indeed verified this statement experimentally for appreciable variations of z from perfect

focus. The reason that this result is interesting is that the diffraction pattern produced by the ground glass is very sensitive to slight displacements of the focusing lens to the extent that large diffraction spots are visible only if the distance z between the ground glass and the lens is very close to the focal length f.

B. Relationship of the Fluctuating Photocurrent to the Fluctuating Field Amplitude

In this section we describe the technique of "self-beating" spectroscopy. In particular, following closely the treatment of G. B. Benedek[13], we derive the relationship between the power density spectrum of the fluctuating photocurrent, measured by this technique, and the power density spectrum of the field amplitude. A schematic representation of the "self-beating" spectrometer is shown in Figure 3. The fluctuating field $E(t)$ produces a fluctuating photocurrent $i(t)$

$$i(t) = G e \beta \frac{c}{8\pi} |E(t)|^2 = G e \beta I(t) \qquad \text{(II.29)}$$

Figure 3

Block diagram of photocurrent power density spectrum measurement apparatus.

E(t), fluctuating field amplitude; P, photomultiplier;

i(t), photocurrent; SA, spectrum analyzer;

$G(\omega)$, photocurrent power spectrum;

R, strip chart recorder

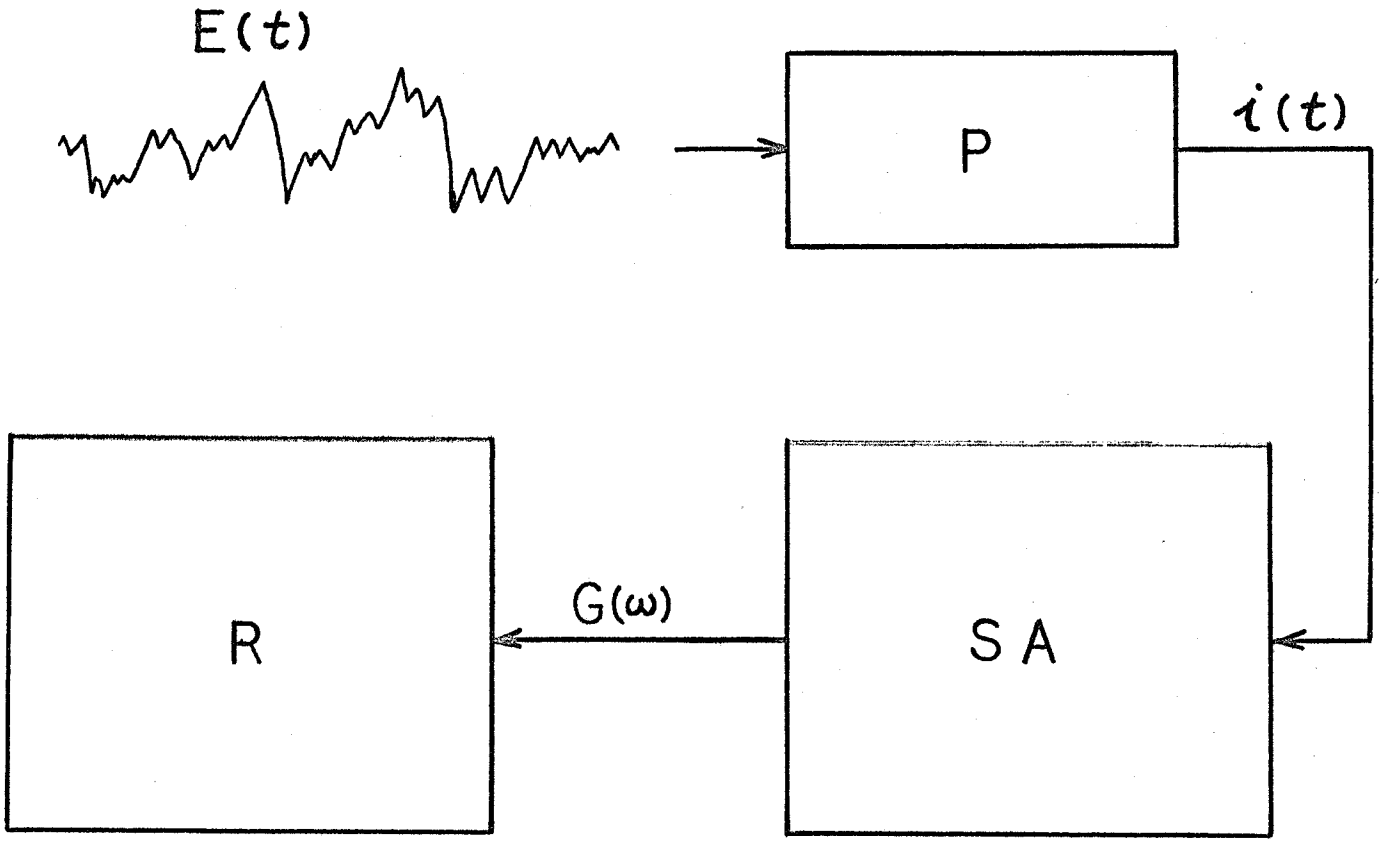
E(t)
P
i(t)
R
G(ω)
S A

which is proportional to the incident field intensity at the photodetector. Here

G = gain of the photomultiplier

e = charge on the electron

β = quantum efficiency of photomultiplier multiplied by area of detector

Thus $\beta I(t)$ is the average number of photoelectrons emitted from the photocathode per second. Here we are assuming that the photomultiplier is illuminated over one coherence area. If such were not the case, we would have to express the intensity as

$$I(t) = \frac{c}{8\pi} \sum_j |E_j(t)|^2 \frac{\Delta A_j}{A} \qquad \text{(II.30)}$$

where ΔA_j denotes the coherence areas

E_j denotes the electric field in each coherence area

A = total detector area.

Considering only a single coherence area, we may use Eq. II.29 as it stands.

According to the Wiener-Khintchine theorem, the power spectrum of the photocurrent is given by

$$G_i(\omega) = \frac{1}{\sqrt{2\pi}} \int_{-\infty}^{\infty} \langle i(t)\, i(t+\tau) \rangle\, e^{-i\omega\tau}\, d\tau . \qquad \text{(II.31)}$$

It can be shown[14] that the photocurrent correlation function may be expressed in terms of the intensity correlation function as

$$\langle i(t) i(t+\tau) \rangle = \beta^2 G^2 e^2 \langle I(t) I(t+\tau) \rangle + G e i_o \delta(\tau) \qquad \text{(II.32)}$$

where i_o is the time average photocurrent. The first term on the right is a consequence of the field intensity fluctuations while the second is a consequence of the sharp pulse nature of the photocurrent and is an approximation to the autocorrelation function for a photocurrent pulse. The representation of this correlation function as a delta function is a good one in this case since the pulses are on the order of 10^{-9} sec. long, while the fluctuations of the field have relaxation times on the order of 10^{-3} seconds.

Using the expression for the intensity of the field in terms of the amplitude, we have

$$\langle i(t)i(t+\tau)\rangle = \left(\frac{\beta G e c}{8\pi}\right)^2 \langle |E(t)|^2 |E(t+\tau)|^2\rangle + Ge\, i_0\, \delta(\tau). \quad \text{(II.33)}$$

Now, if $E(t)$ is a Gaussian random process with zero mean, it can be shown[15] that

$$\langle |E(t)|^2 |E(t+\tau)|^2\rangle = \langle |E(t)|^2\rangle^2 + |\langle E(t)E^*(t+\tau)\rangle|^2. \quad \text{(II.34)}$$

Now denote the correlation functions by:

$$\Gamma(t) = \langle i(t)\, i(t+\tau)\rangle$$

$$\gamma(t) = \langle E(t)\, E^*(t+\tau)\rangle.$$

Then using Eq. II.34, Eq. II.33 becomes

$$\Gamma(\tau) = \left(\frac{\beta G e c}{8\pi}\right)^2 \left(\gamma^2(0) + |\gamma(\tau)|^2\right) + Ge\, i_0\, \delta(\tau). \quad \text{(II.35)}$$

But $$\left(\frac{c}{8\pi}\right)^2 \gamma^2(0) = \left\langle \frac{c}{8\pi} |E(t)|^2\right\rangle^2 = \langle I(t)\rangle^2$$

and thus $$\left(Ge\beta \langle I(t)\rangle\right)^2 = i_0^2, \text{ so}$$

$$\Gamma(\tau) = i_0^2 \left[1 + \frac{|\gamma(\tau)|^2}{|\gamma(0)|^2}\right] + Ge\, i_0\, \delta(\tau). \quad \text{(II.36)}$$

By Eq. II.31, the photocurrent power spectrum is the Fourier transform of Eq. II.36, using Eq. II.26 for $\gamma(\tau)$:

$$G(\omega) = \frac{1}{\sqrt{2\pi}} \int_{-\infty}^{\infty} d\tau \, \Gamma(\tau) \, e^{-i\omega\tau}$$

$$= \frac{1}{\sqrt{2\pi}} \, i_o^2 \, \delta(\omega) + \frac{G e \, i_o}{\sqrt{2\pi}} \tag{II.37}$$

$$+ i_o^2 \left[2v^2\left(\frac{k^2\sigma^2}{f^2} + \frac{1}{4\sigma^2}\right)\right]^{-1/2} \exp\left\{ \frac{-\omega^2}{4v^2\left(\frac{k^2\sigma^2}{f^2} + \frac{1}{4\sigma^2}\right)} \right\} .$$

We note that the spectrum comprises three distinct components: a broad white spectrum due to the shot noise of the photomultiplier, a very high d.c. component due to the average intensity of the incident light and a Gaussian spectrum centered at $\omega = 0$ whose half width is $\sqrt{2}$ times as large as the half width of the field power density spectrum as given by Eq. II.27. Furthermore, the spectrum of Eq. II.37 is centered at $\omega = 0$, whereas the spectrum of Eq. II.27 is centered at the optical frequency of the laser, a region where the inability of conventional

optical methods to measure the small amount of broadening becomes immediately apparent. Thus "self-beating" spectroscopy provides an easily analyzed audio photocurrent while broadening the width of the spectrum by a factor $\sqrt{2}$, itself an aid to better resolution.

C. The Experimental Photocurrent Power Spectra

The measurement of the spectral broadening of the fluctuating field by means of the "self-beating" technique was accomplished in the following way:

The output of the photomultiplier was amplified and chopped electronically at 5000 Hz to displace the spectrum of the photocurrent from the frequency origin, permitting a frequency scan to both sides of the central frequency. This chopped output was then fed to the input of a General Radio Type 1910-A Recording Wave Analyzer. The output was recorded on a strip chart linear in both the frequency (x) axis and the amplitude (or y) axis.

Since the detector of the wave analyzer is a full wave bridge, a linear device, the output yields

the square root of the photocurrent power spectrum[16]. The square root of a Gaussian is still a Gaussian, but with a half-width $\sqrt{2}$ times the original half-width. In addition, there is a factor of $\sqrt{2}$ increase in the measured half-width of the photocurrent spectrum over that of the field power spectrum due solely to the use of the "self-beating" technique, as was shown in the previous section. Thus we expect measurements of the half-width of the frequency broadening, which are scaled off the wave analyzer output, to be a factor of two times the field half-width predicted by Eq. II.28.

To verify the Gaussian nature of the photocurrent spectrum, the shot noise was subtracted from one of our frequency spectra and the resultant spectrum was compared at several points with a Gaussian of the same half-width. The results are presented in Figure 4. Within the limits imposed by the noise, the frequency spectrum is Gaussian as expected.

If we ignore the factor $1/4\sigma^2$ in Eq. II.28, we find that the measured half-width of the photocurrent power spectrum is given by

$$\Delta\nu_{1/2} = \frac{2v}{\lambda f}\,\sigma\sqrt{2\ln 2} \quad \text{Hz}. \qquad \text{(II.38)}$$

Figure 4

Experimental photocurrent spectrum with theoretical Gaussian data points. The peaks at 180 Hz are markers used to center the frequency spectrum. The peak at 0 Hz is due to incomplete suppression of the modulation carrier.

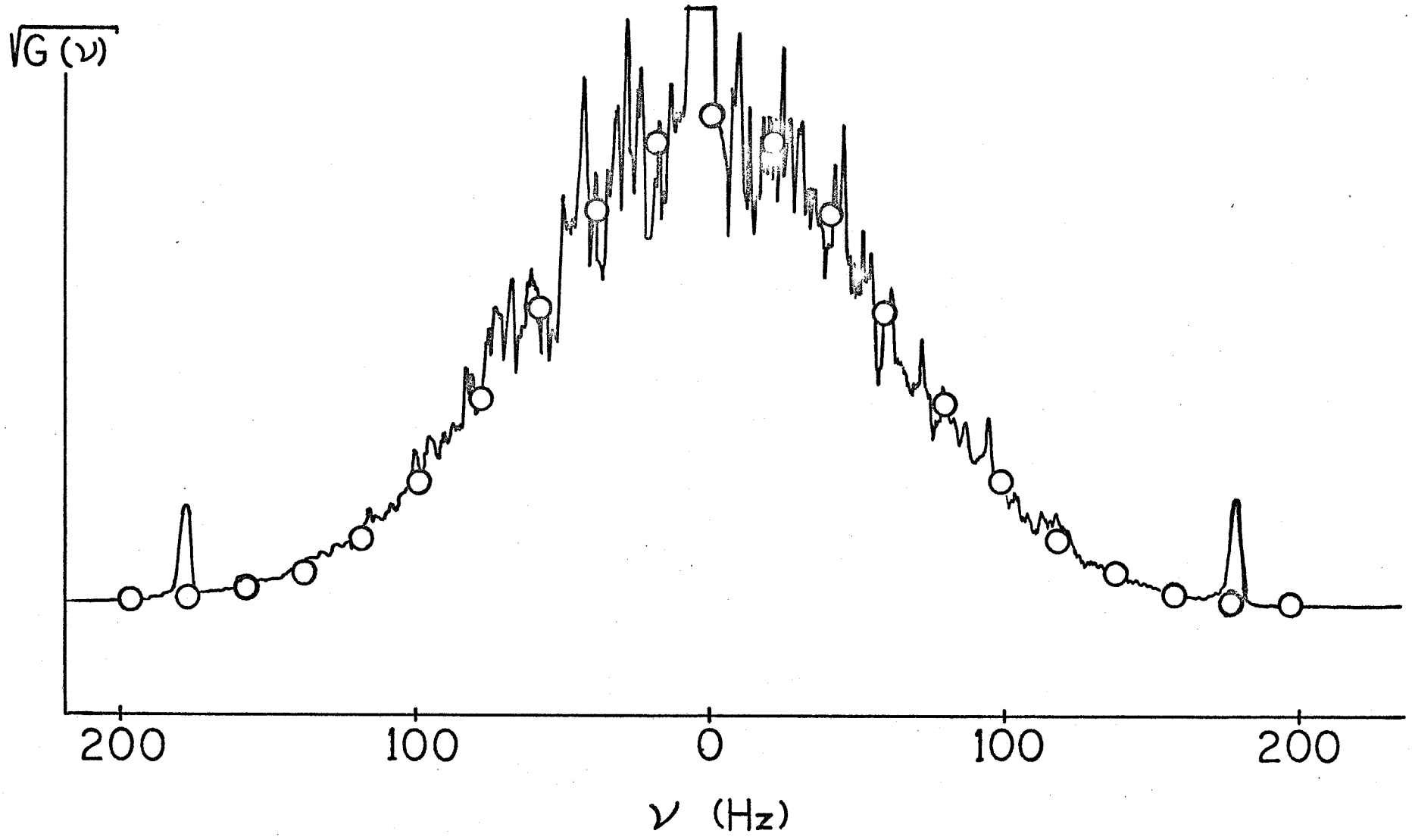
√G (ν)
200
100
0
100
200
ν (Hz)

To verify the dependence of the broadening on the parameters v and f, a number of spectra were run at different focal lengths and velocities. In running the spectra, the wave analyzer bandwidth was set to 3 Hz with the meter response set to SLOW. The spectrum was scanned at the rate of 25 Hz /min. For the broadenings obtained in this experiment, the running of a complete spectrum could take anywhere from 20 minutes to about an hour.

For each given set of experimental parameters, between 3 and 5 spectra were run. The half-widths of these spectra were then determined by the independent visual estimation of several observers and the average and standard deviation of the observations calculated.

The data obtained in this manner is presented graphically in Figures 5 and 6. Figure 5 is a plot of $\Delta\nu_{1/2}$ vs $1/f$ and shows the expected linear relationship in the region where the $1/4\sigma^2$ term can be neglected. Figure 6 shows the predicted linear variation of $\Delta\nu_{1/2}$ with v for three different focal length lenses. In this instance we know that the origin is a physical point, since there is no broadening for zero velocity of the ground glass.

Figure 5

$\Delta \nu_{1/2}$ vs 1/f

$v = 1.329 \text{ cm.sec.}^{-1}$

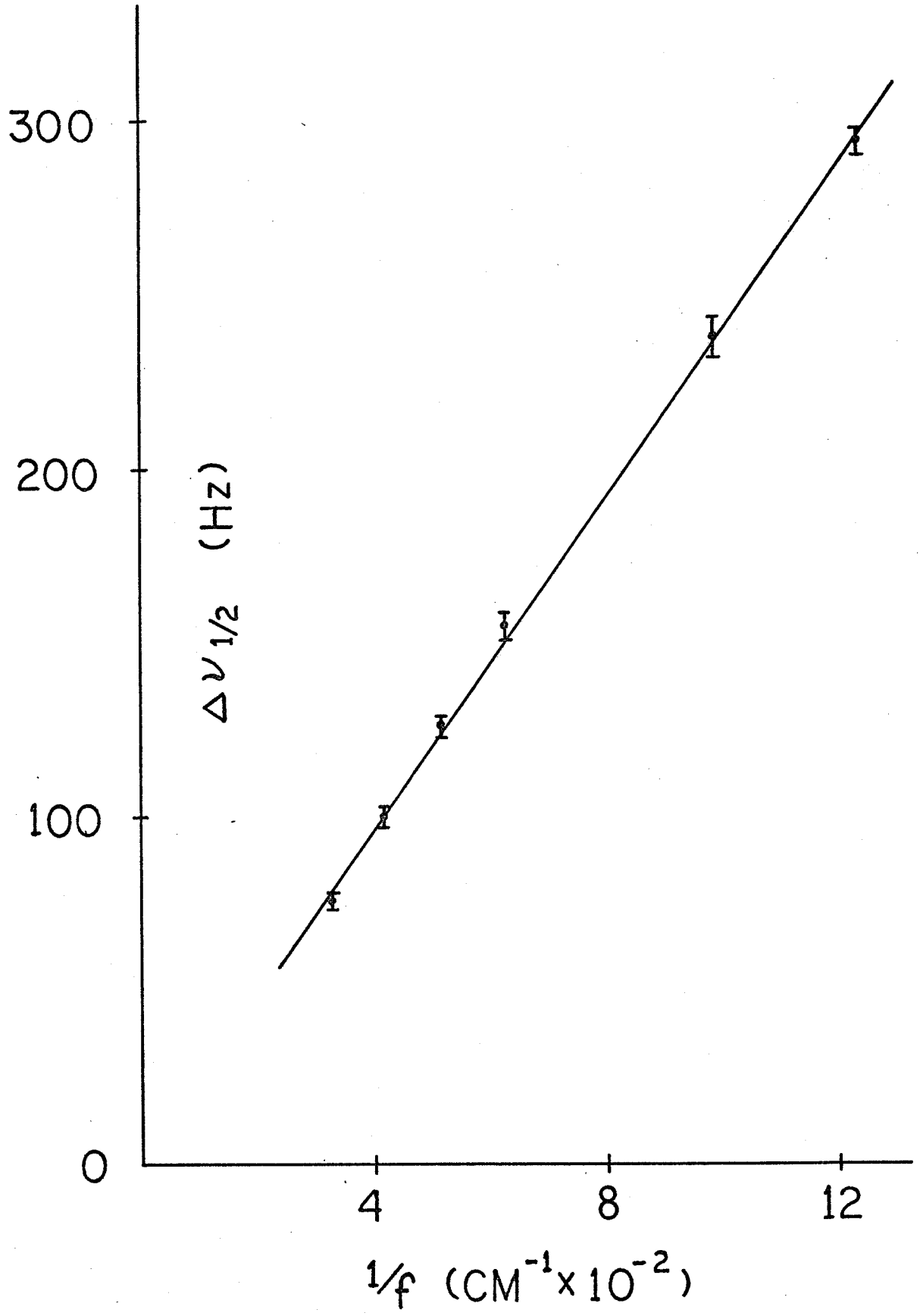
300
200
100
0
$\Delta\nu_{1/2}$ (Hz)
4
8
12
$1/f$ ($CM^{-1} \times 10^{-2}$)

Figure 6

$\Delta \nu_{1/2}$ vs $\frac{1}{f}$

A, f = 10.15 cm

B, f = 11.30 cm

C, f = 19.39 cm

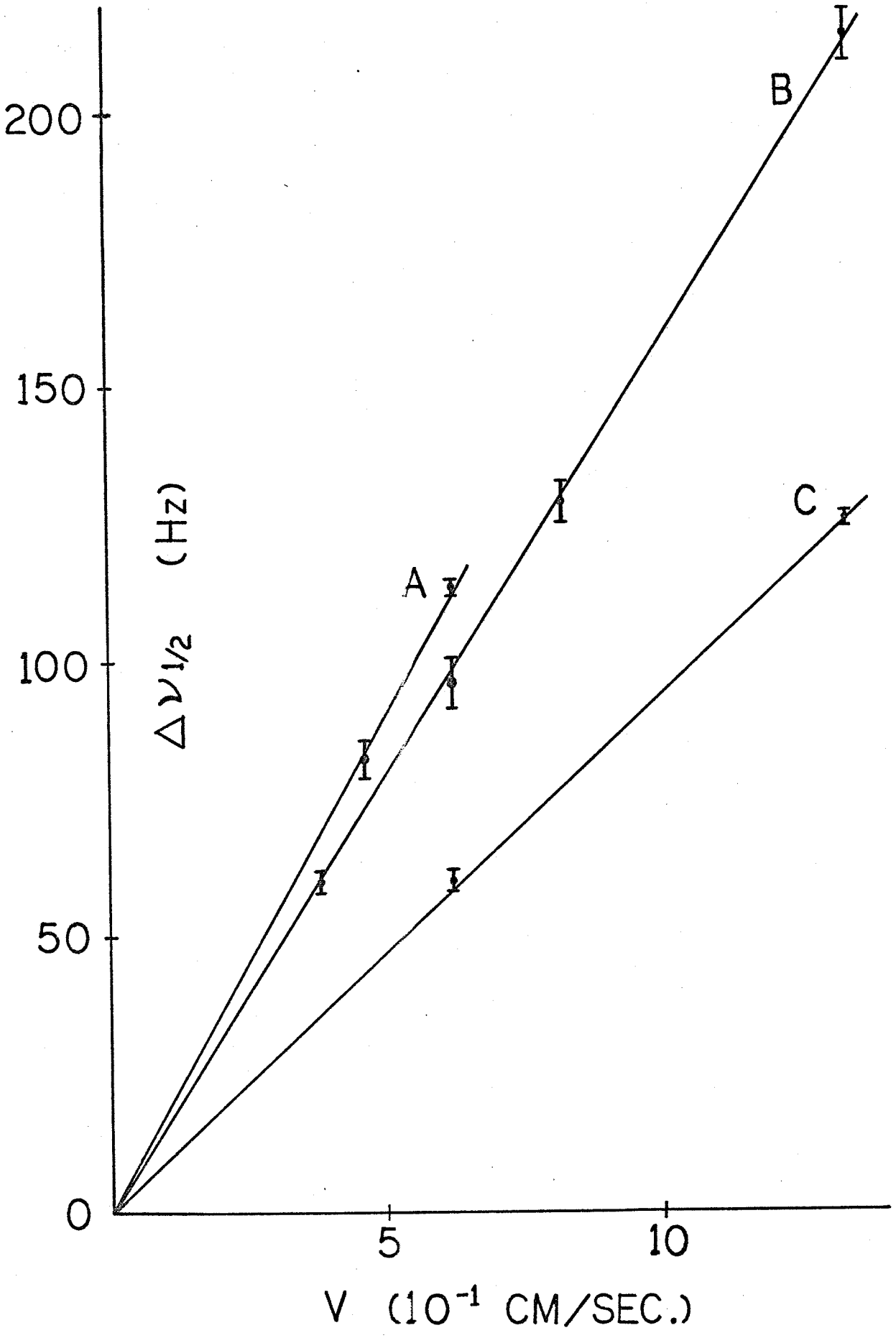
200
150
100
50
0
$\Delta\nu_{1/2}$ (Hz)
A
B
C
5
10
V (10^{-1} CM/SEC.)

The values of σ and f in these results being well known, we can use the data to infer a value of σ for the collimated laser beam. The computed value of .48 mm is in good agreement with the quoted value of .5 mm given by the manufacturer.

The independence of $\Delta\nu_{1/2}$ with scattering angle ψ was verified experimentally up to $\psi = 23^{\circ}$. The decrease in scattered signal at these angles made measurements at scattering angles $>23^{\circ}$ impractical.

The independence of $\Delta\nu_{1/2}$ with respect to z was verified for variations from perfect focus up to 10 per cent of the focal length of a 24 cm focal length lens. For this variation, the size of the focal spot on the ground glass varied in diameter by a factor of roughly 2.5, so that the far field diffraction pattern showed large variations in the size of the diffraction lobes. Beyond the 10 per cent variation, some change in $\Delta\nu_{1/2}$ became apparent. We believe that this is due to the appearance of errors in approximations made in the derivation of the Fresnel diffraction formula, Eq. II.3.

III. PHOTOCOUNT STATISTICS

A. Theoretical Formalism

The subject of photoelectron counting distributions has been well explored in many places.[17] As a convenience to the reader, therefore, it will suffice to provide a very brief synopsis of the semiclassical formalism of Mandel.[18]

Starting from a first order perturbation theory treatment of the interaction between the light field and the detector, the probability $P(n,T)$ of counting n photoelectrons in an interval T which is very short compared with the coherence time $1/\Delta\nu$, and for one mode of the optical field, is given by

$$P(n, T \ll 1/\Delta\nu) = \int_0^\infty P(I) \frac{(\alpha I)^n}{n!} e^{-\alpha I} \, dI \qquad \text{(III.1)}$$

where: I = classical light intensity at detector

$P(I)$ = probability distribution for I

$\alpha = \beta T$ = product of quantum efficiency times detector area times counting interval.

In the event that counting is done for periods T exceeding the coherence time of the field, the result becomes

$$P(n,T) = \int_0^\infty P(W) \frac{(\beta W)^n}{n!} e^{-\beta W} \, dW \qquad \text{(III.2)}$$

where

$$W = \int_{t'}^{t'+T} I(t) \, dt \, .$$

A number of interesting properties of this distribution are tabulated in Appendix A of Dr. William Clark's thesis.[19]

B. The Field Amplitude Probability Distribution and its Counting Statistics

Since we are following the semiclassical theory of photoelectron counting statistics due to Mandel, we present in this section a classical derivation of the probability distribution for the amplitude of the field scattered from a stationary ground glass. The argument is essentially that of Lord Rayleigh,[20] who treats the

problem of a random superposition of acoustical vibrators. In the context of the quantum mechanical theory, Glauber[21] presents a more elegant derivation which leads to a Gaussian $P(\alpha)$.

We begin by assuming a very simple model for the scattering of the constant intensity incident beam and the detection of the scattered field. In Figure 7 there are, within the illuminated area on the ground glass A, a number m of equal strength scattering centers s, whose phases and positions are uncorrelated. At the detection point P, some distance away, the detected field is then the superposition of a number of equal amplitude fields whose phases are random. Lack of any a priori information leads us to take the phases of the fields at the detection point as being uniformly distributed over $(0, 2\pi)$. For simplicity we take the amplitudes of the fields at the detector to be equal to one.

Consider an ensemble consisting of M of these m scatterer systems. At the detection point, each system in the ensemble has a resultant amplitude r and a phase θ. Now we consider an (x,y) plane, Figure 8.

Any point in this plane represents a possible system realization. What we are after is the ensemble

Figure 7

Simple model for scattering from ground glass.
A, illuminated area;
s, unit amplitude scattering center;
D, detector.

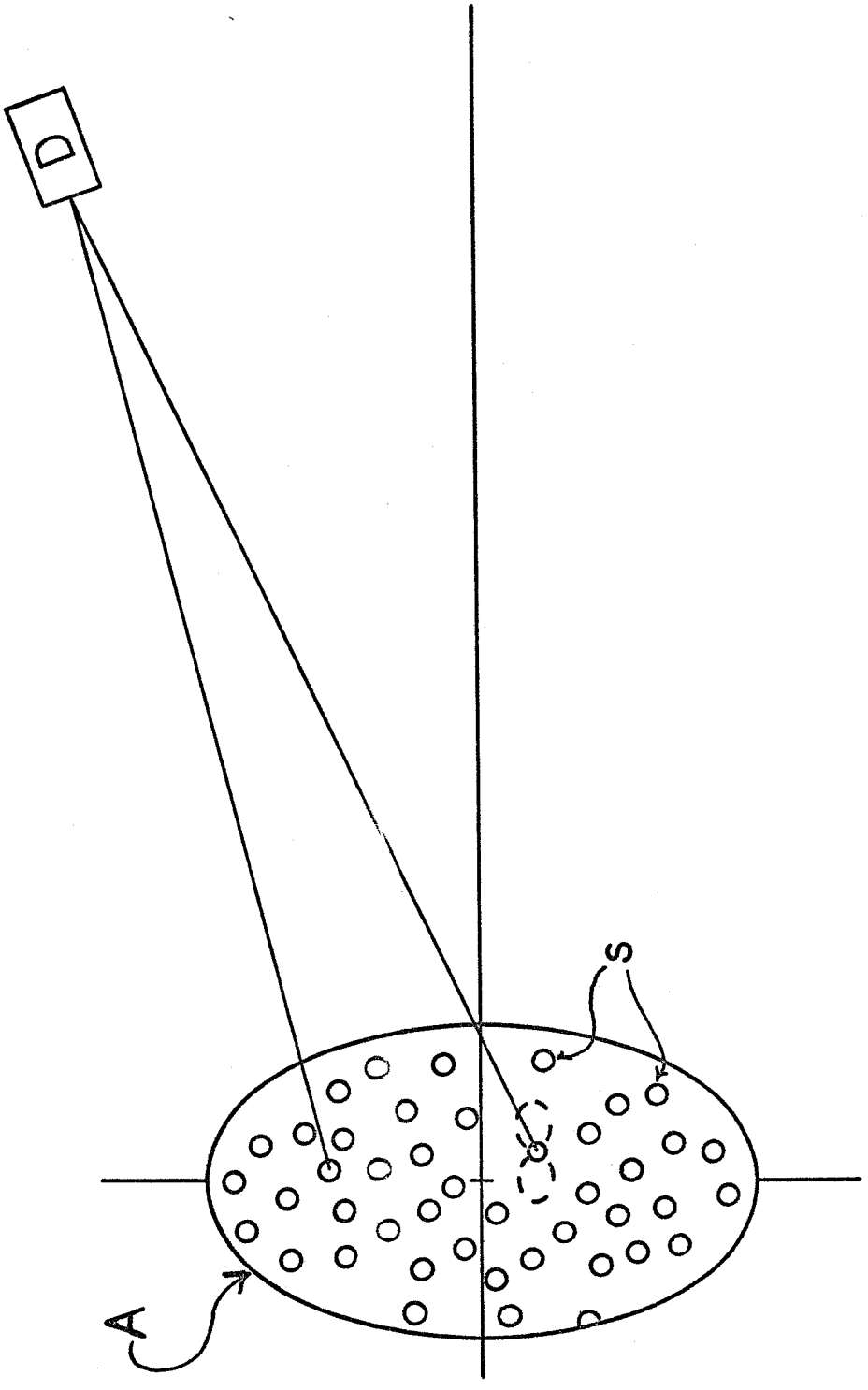
D
S
A

Figure 8

(X,Y) plane for amplitude and phase.

(x',y'), end point of m scatterer system

(x,y), end point of m + 1 scatterer system

l, amplitude of additional scatterer

φ, phase of additional scatterer

r, amplitude of m + 1 scatterer system

ϑ, phase of m + 1 scatterer system

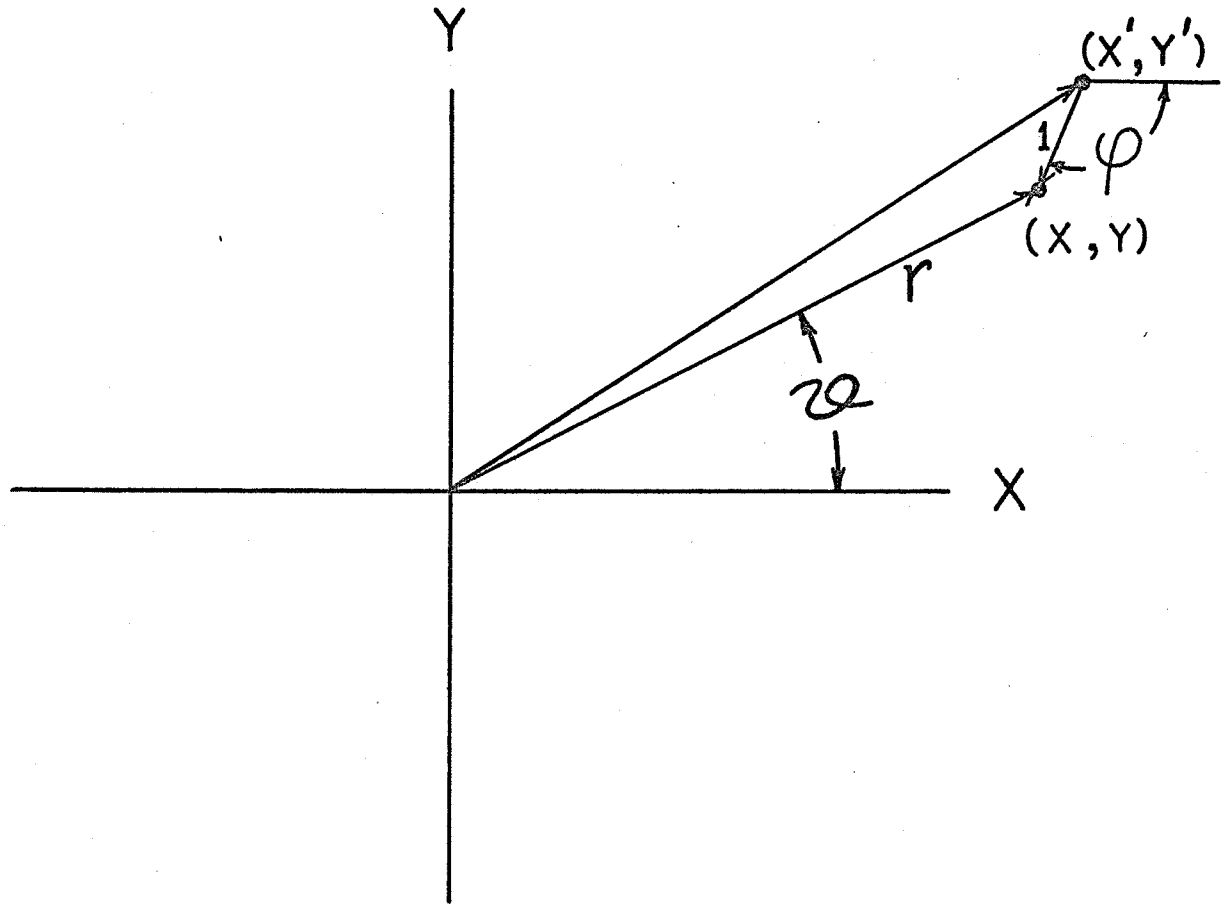
Y
(X', Y')
1
φ
(X , Y)
r
ϑ
X

density function $f(m, x, y)$ for the distribution of these points in the plane. From our assumption that the phases of the contributions at the detection point are uniformly distributed, we know that the distribution will be independent of ϑ.

We assume that $Mf(m, x, y)$ systems in the ensemble are found to have their resultant amplitude and phase within dxdy. We ask how the addition of one random phase unit scatterer to each system in the ensemble changes the distribution function.

To end up at (x, y), the system must have started at $x' = x - \cos\varphi$, $y' = y - \sin\varphi$, where φ is the phase of the additional unit amplitude at the detection point. Now φ is uniformly distributed with a density $1/2\pi$. The number of ensemble members to be found within dxdy is, therefore,

$$M\,dx\,dy \int_0^{2\pi} f(m, x-\cos\varphi, y-\sin\varphi)\,\frac{d\varphi}{2\pi} \quad . \qquad \text{(III.3)}$$

But this is also equal to $Mf(m + 1, x, y)dxdy$. We have, therefore, the relationship

$$f(m+1,x,y) = \int_0^{2\pi} f(m,x',y') \frac{d\varphi}{2\pi} . \qquad \text{(III.4)}$$

Expanding f(m, x', y') in a Taylor Series, we have

$$f(m,x',y') = f(m, x-\cos\varphi, y-\sin\varphi)$$

$$= f(m,x,y) + \frac{\partial f}{\partial x}(-\cos\varphi) + \frac{\partial f}{\partial y}(-\sin\varphi) \qquad \text{(III.5)}$$

$$+ \frac{1}{2}\frac{\partial^2 f}{\partial x^2}\cos^2\varphi + \frac{\partial^2 f}{\partial x\,\partial y}\cos\varphi\sin\varphi + \frac{1}{2}\frac{\partial^2 f}{\partial y^2}\sin^2\varphi + \cdots$$

Using Eq. III.5 in Eq. III.4, we arrive at the result

$$f(m+1,x,y) = f(m,x,y) + \frac{1}{4}\frac{\partial^2 f}{\partial x^2} + \frac{1}{4}\frac{\partial^2 f}{\partial y^2} + \cdots \qquad \text{(III.6)}$$

For M very large, we let $1 = \delta m$ and obtain the approximate differential equation

$$\frac{\partial f}{\partial m} = \frac{1}{4}\left(\frac{\partial^2 f}{\partial x^2} + \frac{\partial^2 f}{\partial y^2}\right) . \qquad \text{(III.7)}$$

Equation III.7 is in the form of a two dimensional diffusion equation. We can determine the initial condition by noting that for no scatterers we require (looking only at the scattered field)

$$f(0,x,y) = \delta(x)\delta(y) . \qquad \text{(III.8)}$$

The solution of Eq. III.7 is easily accomplished using a partial Fourier Transform technique.[22] We let

$$F(m,k_1,k_2) = \frac{1}{2\pi}\int_{-\infty}^{\infty}\int f(m,x,y)\, e^{ik_1x}\, e^{ik_2y}\, dx\, dy \qquad \text{(III.9)}$$

and assume the validity of differentiation with respect to m under the integral sign;

$$\frac{dF}{dm} = \frac{1}{2\pi}\int_{-\infty}^{\infty}\int \frac{\partial f}{\partial m}\, e^{ik_1x}\, e^{ik_2y}\, dx\, dy . \qquad \text{(III.10)}$$

Integration by parts, furthermore, gives us the relation

$$\frac{1}{2\pi}\int_{-\infty}^{\infty}\int \frac{\partial^2 f}{\partial x^2}\, e^{ik_1 x}\, e^{ik_2 y}\, dx\, dy = -k_1^2 F(m,k_1,k_2) \qquad \text{(III.11)}$$

with a similar result for $\partial^2 f/\partial y^2$. Then F(m, k_1, k_2) satisfies the ordinary differential equation,

$$\frac{dF(m,k_1,k_2)}{dm} = -\frac{(k_1^2+k_2^2)}{4} F(m,k_1,k_2) \qquad \text{(III.12)}$$

so

$$F(m,k_1,k_2) = F(0,k_1,k_2)\, e^{-\frac{(k_1^2+k_2^2)}{4} m} . \qquad \text{(III.13)}$$

By the initial condition,

$$F(0,k_1,k_2) = \frac{1}{2\pi}\int_{-\infty}^{\infty}\int \delta(x)\,\delta(y)\, e^{i(k_1 x + k_2 y)}\, dx\, dy = \frac{1}{2\pi} . \qquad \text{(III.14)}$$

Thus

$$F(m,k_1,k_2) = \frac{1}{2\pi}\, e^{-\frac{(k_1^2+k_2^2)}{4} m} . \qquad \text{(III.15)}$$

The inverse transform of Eq. III.15 is easily performed to yield

$$f(m,x,y) = \frac{1}{\pi m}\, e^{-\frac{x^2+y^2}{m}} , \qquad \text{(III.16)}$$

a Gaussian distribution with zero mean.

The probability that the field amplitude falls between r and r + dr is given by

$$\frac{1}{\pi m}\int_0^{2\pi} e^{-\frac{x^2+y^2}{m}}\,dx\,dy \;=\; \frac{1}{\pi m}\int_0^{2\pi} e^{-r^2/m}\,r\,dr\,d\varphi$$

or
$$P(r)\,dr \;=\; \frac{2}{m}\; e^{-r^2/m}\; r\,dr\,. \qquad \text{(III.17)}$$

For the probability in intensity, one uses

$$P(r)\,dr \;=\; P(I)\,dI\,, \qquad \text{(III.18)}$$

with $I = r^2$, to obtain

$$P(I) \;=\; \frac{e^{-I/m}}{m}\,. \qquad \text{(III.19)}$$

The average intensity at the detection point is

$$\langle I\rangle = \int_0^{\infty} I\,P(I)\,dI \;=\; \int_0^{\infty} I\,\frac{e^{-I/m}}{m} \;=\; m\,,$$

so
$$P(I) \;=\; \frac{e^{-I/\langle I\rangle}}{\langle I\rangle}\,. \qquad \text{(III.20)}$$

To put this in contact with the realities of the experiment, we use the ergodic theorem to assert that the probability density derived on the basis of an ensemble average holds true for one system evolving in time in a stationary manner. The time evolution is obtained by merely rotating the ground glass. It is easy to visualize that if one samples the field at the detection point at instants of time separated by a period of time long enough to insure a new random pattern of scatterers in the illuminated region, the resulting probability distribution will be given by Eq. III.20.

We may thus use Eq. III.20 as the P(I) in Mandel's formula (Eq. III.1) under the proviso that we sample for a period of time much less than that during which an appreciable change in the scattering situation takes place; in other words shorter than the relaxation time of the scatterer. Similarly, we are required to sample at intervals separated by more than the relaxation time. Substitution of this P(I) in Mandel's formula gives

$$P(n,T) = \int_0^\infty \frac{e^{-I/\langle I\rangle}}{\langle I\rangle} \frac{(\beta I T)^n}{n!} e^{-\beta I T} dI . \qquad \text{(III.21)}$$

This integral is easily evaluated to give

$$P(n,T) = \frac{\langle n \rangle^n}{(1+\langle n \rangle)^{n+1}} \qquad \text{(III.22)}$$

which is a Bose-Einstein distribution with $\langle n \rangle = \beta T \langle I \rangle$. For this distribution, the reduced factorial moments H_2 and H_3, defined as

$$H_2 = \frac{\langle n^2 \rangle - \langle n \rangle - \langle n \rangle^2}{\langle n \rangle^2}$$

$$H_3 = \frac{\langle n^3 \rangle - 3\langle n^2 \rangle + 2\langle n \rangle - \langle n \rangle^3}{\langle n \rangle^3}, \qquad \text{(III.23)}$$

are easily shown to take the values $H_2 = 1.000$ and $H_3 = 5.000$.

C. The Photocount Experiment

To confirm the validity of the assumption of zero mean Gaussian field statistics, a photocount experiment was constructed. A block diagram of the

experiment and the photocount apparatus appears in Figure 9. A more detailed description of the system, as well as operating instructions and schematics, is given in Appendix A.

In Figure 9, light from the collimated laser L is focused by lens f onto the ground glass GG. The lens is adjusted for perfect focus by observing the size of the diffraction spots in the far field and maximizing the size of these spots. This insures that we have the largest possible coherence areas commensurate with the focal length lens being used. The glass itself is in the form of a disk 9 inches in diameter. It is centered on an axle which can be belt driven by a synchronous clock motor (1 rpm). Assorted pulleys are available to provide a range of rotary speeds for the glass. The laser beam is focused to a spot approximately 9.5 cm from the axis of rotation. Liberal use was made of black velvet and cardboard baffles to limit the possibility that stray light could fall on the detector.

The diffraction pattern from the ground glass is sampled at a point in the far field by a photomultiplier P. Two photomultipliers were used in the course of the

Figure 9

Photon counting system block diagram.

L, laser; f, focusing lens; GG, ground glass;

P, photomultiplier; A, wide band amplifier;

S, Lecroy 520A scaler; G1, Advanced Automation 2000 generator; G2, Hewlett-Packard 222A generator;

I, computer-system interface; C, PDP-8/L computer.

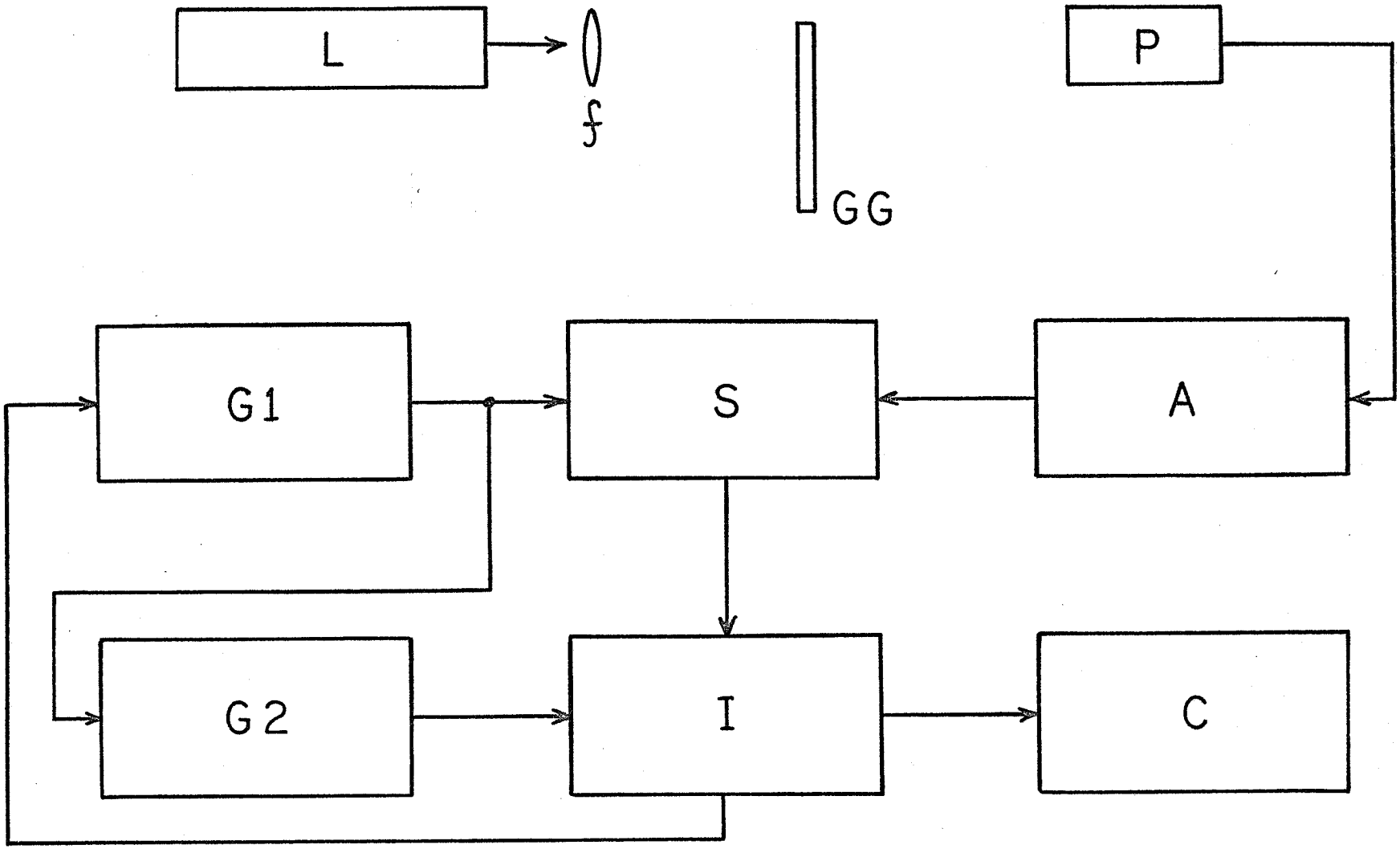
L
f
GG
P
G1
S
A
G2
I
C

experiment, an RCA 1P28 and a Phillips XP1021. The initial experiments were done with the 1P28, which has a lower dark noise. Unfortunately, as the experiment progressed, this PMT appeared to give increasing numbers of noise counts which were correlated with the signal. This type of correlated noise cannot be separated from the data by the technique of deconvolving the noise and signal distribution.[23] For this reason, the XP1021 was used for later measurements and showed no tendency to correlated counts. Both photomultipliers were equipped with 6328A° bandpass filters and approximately 1 mm apertures to insure that field sampling was done well within a coherence area.

The output of the photomultiplier, in the form of narrow current pulses, is amplified by A and counted in a 200 mHz scaler S . The time during which S can count pulses is controlled by the duration of the output pulse of generator G1. The trailing edge of this pulse triggers generator G2 which initiates read in of the number of counts in S into the computer C through the interface I . After read in, the interface sends a trigger pulse to G1 which starts the counting sequence again. The dead time of the system (time following a

pulse which is counted during which an additional pulse will not be counted) is essentially determined by the frequency response of the scaler, and is on the order of 5 nanoseconds.

The computer is programmed to function as a 512 channel storage device. The channels correspond to 0, 1, 2, ..., 511 possible counts per counting interval T. When the computer receives a given count number from S which is less than 511, it increments the number in the computer memory at a location corresponding to the given count. It thus records the number of times a given count occurs up to a maximum of 8.4×10^6 occurrences per count.

When a count channel overflows, or the operator so desires, the computer will calculate and print out all the count probabilities as well as the mean and mean squared number of counts. It also prints out the reduced factorial moments H_2 and H_3 as well as the total number of sample intervals occurring in the course of the experiment.

Subsequent to the termination of the counting experiment, the actual photocount distribution can be determined by a previously described technique.[23] This

technique essentially deconvolves the experimentally determined probability distribution and the known counting distribution of the photomultiplier noise. In actual practice, this procedure was found to be unnecessary in most cases, since the 512 channel capability of the counting system allowed operation, in most cases, at an average number of signal counts per counting interval that surpassed the noise count by many orders of magnitude without running into appreciable dead time effects. In general, we used the rule of thumb given by Arecchi[24] that dead time effects begin to become appreciable when

$$n_{max} \cdot \frac{\tau}{T} \approx \frac{1}{100} . \qquad \text{(III.24)}$$

Here n_{max} = highest count number recorded
T = length of counting interval
τ = dead time $\approx 5 \times 10^{-9}$ sec.

Thus, for a 50 μsec counting interval, we require $n_{max} < 100$ counts.

Some idea of the necessity for the processing of the experimental data may be obtained by calculating

the effects on the moments of the distribution due to the presence of the noise. For this purpose we rely on some properties of the cumulants of independent probability distributions.[25]

We begin with the characteristic function of a random variable (in this case taken to be discrete)

$$\varphi(t) = \sum_{n=0}^{\infty} P(x_n)\, e^{itx_n} . \qquad \text{(III.25)}$$

We now define the cumulants K_n as

$$\ln \varphi(t) = \sum_{n=0}^{\infty} K_n \frac{(it)^n}{n!} . \qquad \text{(III.26)}$$

Now for two independent distributions,[26]

$$\varphi(t) = \varphi_1(t)\, \varphi_2(t) , \qquad \text{hence}$$

$$\ln \varphi(t) = \ln \varphi_1(t) + \ln \varphi_2(t) = \sum_{n=0}^{\infty} \left(K_n^{(1)} + K_n^{(2)}\right) \frac{(it)^n}{n!}$$

$$= \sum_{n=0}^{\infty} K_n \frac{(it)^n}{n!} .$$

Thus $$K_n = K_n^{(1)} + K_n^{(2)} . \qquad \text{(III.27)}$$

The first 3 cumulants are, for $x_n = n$

$$\begin{aligned} \kappa_1 &= \langle n \rangle \\ \kappa_2 &= \langle (n - \langle n \rangle)^2 \rangle \\ \kappa_3 &= \langle (n - \langle n \rangle)^3 \rangle \quad . \end{aligned} \tag{III.28}$$

In terms of the parameters which appear in the printout of the computer,

$$\begin{aligned} \kappa_1 &= \langle n \rangle \\ \kappa_2 &= \langle n \rangle^2 H_2 + \langle n \rangle \\ \kappa_3 &= \langle n \rangle^3 H_3 + 3\langle n \rangle^2 H_2 (1 - \langle n \rangle) + \langle n \rangle \quad . \end{aligned} \tag{III.29}$$

Using Eqs III.29 in conjunction with III.27, we can estimate the effect of the (known) noise on the actual distribution. Thus, if we use superscripts E,N,S to denote respectively experimental, noise, and signal parameters, and assume the signal and noise counts are uncorrelated, we may write

$$\langle n^S \rangle = \langle n^E \rangle - \langle n^N \rangle$$

$$H_2^S = \left[\langle n^E \rangle^2 H_2^E - \langle n^N \rangle^2 H_2^N \right] \frac{1}{\langle n^S \rangle^2}$$

$$H_3^S = \left[\langle n^E \rangle^3 H_3^E - 3\langle n^E \rangle^3 H_2^E - \langle n^N \rangle^3 H_3^N + 3\langle n^N \rangle^3 H_2^N + 3\langle n^S \rangle^3 H_2^S \right] \frac{1}{\langle n^S \rangle^3} \qquad \text{(III.30)}$$

From Eqs. III.30, it can be seen that if the noise count mean number is small with respect to the experimental count mean number, the experimental parameters will closely approximate the true signal parameters.

As an example, for an actual experimental case with

$$\langle n^E \rangle = 3.820 \quad , \quad H_2^E = 1.005, \quad H_3^E = 5.006$$

$$\langle n^N \rangle = 0.00098, \quad H_2^N = 20.73, \quad H_3^N = -1.00$$

the signal parameters, using Eqs. III.30, are found to be

$$\langle n^S \rangle = 3.819 \quad , \quad H_2^S = 1.006, \quad H_3^N = 5.009.$$

An actual separation of the signal from the experimental data showed that the probabilities differed only in the fourth decimal place. In such a case, therefore, the separation is not necessary. For smaller mean

numbers, of course, such is not the case. In treating the data presented herein, most data was obtained with sufficient signal to obviate the need for unraveling the noise. For the data which needed unraveling, a program similar to Dr. John Kuppenheimer's PHOTON 2[27] was written in assembler language for the PDP-8/L and used to determine the actual signal count probabilities.

D. Experimental Results; 1 micron Ground Glass

According to the theory presented in section III.B, the field amplitude probability distribution is a Gaussian function for every value of the translational speed and for all scattering angles and focal lengths. Thus we expect a Bose-Einstein distribution of photo-counts to be found independent of variations in v, f, and Ψ.

Preparatory to experimental verification of this independence, some assurance was needed that the incident laser veam was truly of constant intensity. The laser used in the experiment, a Spectra-Physics Model 119 He-Ne laser, has been used at WPI in photon counting experiments over a period of several years.[28] The

stability of its output intensity has thus been well documented. As further evidence we present the data from one stability run on this laser which was made preparatory to a scattering experiment.

For a constant intensity laser, $P(I) = \delta(I)$. Upon substitution of this $P(I)$ into Mandel's formula, Eq. III.I, one finds a Poisson distribution for the predicted $P(n, T)$;

$$P(n,T) = \frac{\langle n \rangle e^{-\langle n \rangle}}{n!} \qquad \text{(III.31)}$$

where $\langle n \rangle = \beta I T$.

The Poisson distribution has the property that

$H_2 = H_3 = 0.0$.

In Table I, we present an experimental distribution obtained by counting on the output of the 119 laser, together with a theoretical Poisson distribution with the same mean number as the experimental distribution. The error column in Table I is computed by using the knowledge that the standard deviation in a measurement of a number of counts N_n is given by $\sqrt{N_n}$.[29] The true probability is therefore

$$P(n) \simeq \frac{N_n \pm \sqrt{N_n}}{N_T} = P_E(n)\left(1 + \frac{1}{\sqrt{N_n}}\right) \qquad \text{(III.32)}$$

Table I.

Counting Distribution, 119 Laser.

NBAR +0.347834E+01

N2BAR +0.155639E+02

H2 -.109777E-02

H3 -.285059E-02

NO. OF EVENTS 3.17E+06		Poisson	Error
P(000)	+0.302156E-01	0.308586E-01	0.986914E-04
P(001)	+0.107874E+00	0.107337E+00	0.184063E-03
P(002)	+0.185722E+00	0.186677E+00	0.242737E-03
P(003)	+0.218580E+00	0.216442E+00	0.261374E-03
P(004)	+0.186606E+00	0.188215E+00	0.243735E-03
P(005)	+0.132034E+00	0.130935E+00	0.203292E-03
P(006)	+0.754939E-01	0.759060E-01	0.154785E-03
P(007)	+0.378937E-01	0.377181E-01	0.109111E-03
P(008)	+0.161812E-01	0.163996E-01	0.719462E-04
P(009)	+0.627511E-02	0.633814E-02	0.447273E-04
P(010)	+0.216840E-02	0.220462E-02	0.263790E-04
P(011)	+0.677350E-03	0.697129E-03	0.148337E-04
P(012)	+0.204530E-03	0.202071E-03	0.798626E-05
P(013)	+0.530264E-04	0.540671E-04	0.413103E-05
P(014)	+0.126253E-04	0.134331E-04	0.205911E-05
P(015)	+0.473450E-05	0.311500E-05	0.991563E-06
P(016)	+0.631267E-06	0.677189E-06	0.462324E-06
P(017)	+0.000000E+00	0.138559E-06	0.209126E-06
P(018)	+0.000000E+00	0.267752E-07	0.919301E-07
P(019)	+0.000000E+00	0.490175E-08	0.393339E-07

where N_T is the total number of events and $P_E(n)$ is the experimentally determined probability. Since $N_n \approx P(n)\ N_T$, we have

$$P(n) \simeq P_E(n) \pm \sqrt{\frac{P(n)}{N_T}} \quad . \qquad \text{(III.33)}$$

Here P(n) is the calculated theoretical probability distribution. The quantity under the square root sign is listed under the ERROR column in Table I.

We see in Table I that, despite the fact that the factorial moments are not quite equal to zero, the experimental probabilities agree with the theoretical distribution to within the third decimal place until the counting errors become appreciable. The distribution is, in fact, one of the poorer ones in regard to the reduced factorial moments, most experimental values of H_2 and H_3 being about an order of magnitude smaller. The distribution, nevertheless, is Poisson to a high degree of precision. This is shown graphically in Figure 10, where the agreement over 5 decades is readily apparent. The error bars on this Figure derive from the counting error associated with finite statistics as previously discussed. The error bars only appear on the last two data points since in the other cases they are smaller than the size of the dots used to denote the experimental points.

Figure 10

Counting distribution of 119 laser. The points represent the experimental data while the solid line is a theoretical Poisson distribution with the same mean number.

Counting interval = 25 μsec.

Off time = 100 μsec.

Number of events = 3.1^{-} x 10^{6}

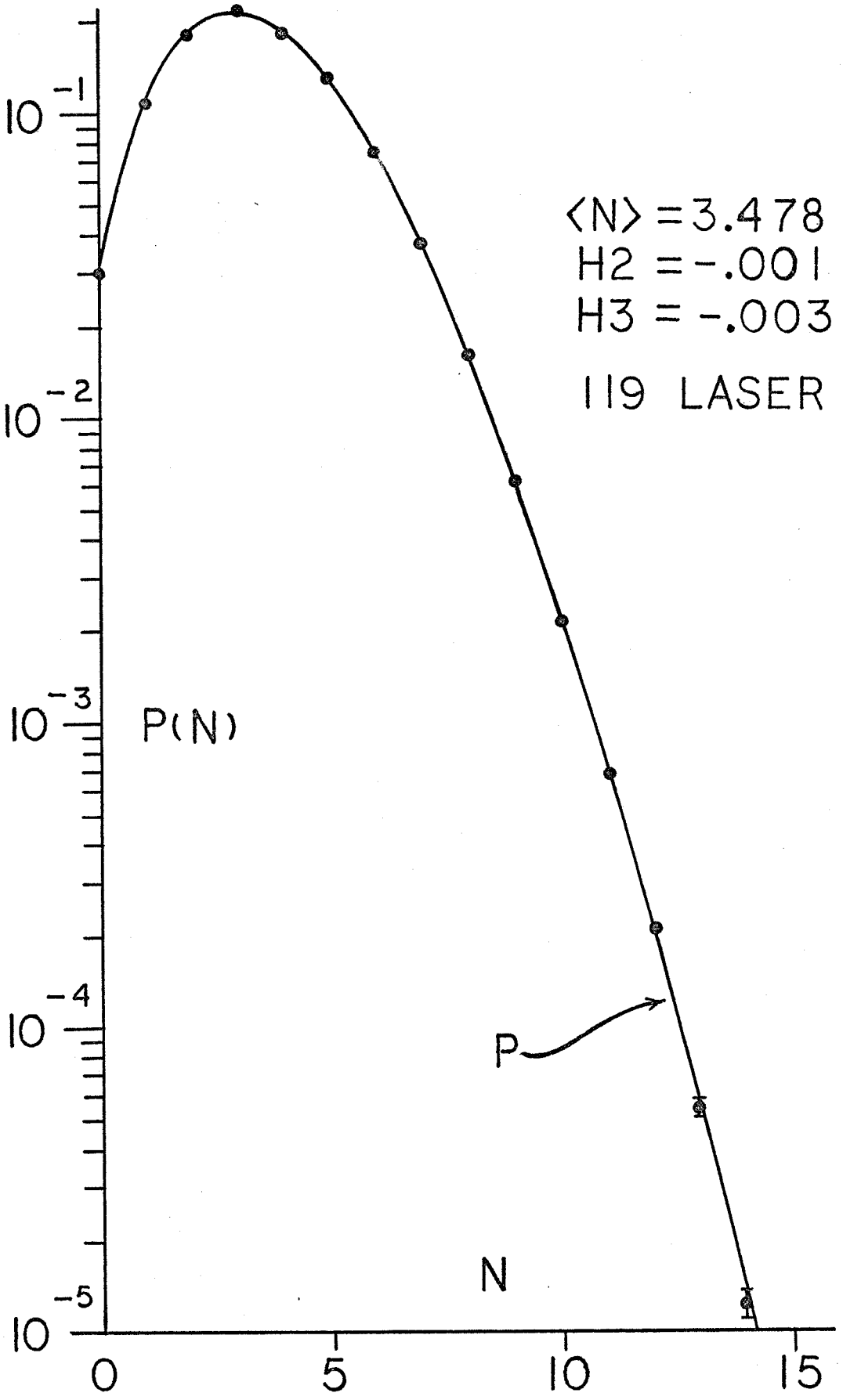
10^-1
10^-2
10^-3
10^-4
10^-5
P(N)
<N> = 3.478
H2 = -.001
H3 = -.003
119 LASER
P
N
0
5
10
15

In Table II, we present an output of the program which separates the signal count probabilities from the experiment and noise data. The effect on the probability distribution in this case is negligible.

The experimental photocount data, for the case of light scattered from a rotating ground glass with approximately 1 micron inhomogeneities, is presented in Tables III, IV and V. The reduced factorial moments H_2 and H_3, which are given for each case, may be compared with the theoretical values: $H_2 = 1.000$ and $H_3 = 5.000$ for a Bose-Einstein distribution. The invariance of the photocount statistics with respect to the parameters v, f and ψ (the linear velocity of the ground glass, the focal length of the focusing lens and the angle of scattering respectively) is clearly demonstrated. As an additional check, a theoretical Bose-Einstein distribution with counting errors was generated for each value of $\langle n \rangle$ obtained experimentally. The experimental probabilities, P(n), were observed to agree with the theoretical distributions within the errors to be expected from the finiteness of the statistics. Graphical comparisons of two of the experimental distributions with their respective theoretical distributions are given in Figures 11 and 12.

Table II.

Signal Unraveler Output

Experiment		Signal	
PE(000)	.302156E-01	PS(000)	.303274E-01
PE(001)	.107874E+00	PS(001)	.108167E+00
PE(002)	.185722E+00	PS(002)	.186026E+00
PE(003)	.218580E+00	PS(003)	.218720E+00
PE(004)	.186606E+00	PS(004)	.186498E+00
PE(005)	.132034E+00	PS(005)	.131829E+00
PE(006)	.754939E-01	PS(006)	.752738E-01
PE(007)	.378937E-01	PS(007)	.377416E-01
PE(008)	.161812E-01	PS(008)	.160910E-01
PE(009)	.627511E-02	PS(009)	.623214E-02
PE(010)	.216840E-02	PS(010)	.214988E-02
PE(011)	.677350E-03	PS(011)	.670246E-03
PE(012)	.204530E-03	PS(012)	.202081E-03
PE(013)	.530264E-04	PS(013)	.521755E-04
PE(014)	.126253E-04	PS(014)	.123551E-04
PE(015)	.473450E-05	PS(015)	.465773E-05
PE(016)	.631267E-06	PS(016)	.598202E-06
SUM	.999999E+00	SUM	.999999E+00
NBAR	.347833E+01	NBAR	.347439E+01
N2BAR	.155639E+02	N2BAR	.155319E+02
H2	-.109580E-02	H2	-.115359E-02
H3	-.284788E-02	H3	-.303658E-02

Noise

PN(000)	.996314E+00
PN(001)	.347921E-02
PN(002)	.168988E-03
PN(003)	.254532E-04
PN(004)	.865933E-05
PN(005)	.183682E-05
PN(006)	.524807E-06
PN(007)	.262404E-06
PN(008)	.000000E+00
PN(009)	.262404E-06
SUM	.999998E+00

Table III. Independence of statistics with speed.

f = 19.39 cm. $\Psi = 0$

Exp. #	linear velocity (cm/sec.)	$\langle n \rangle$	H_2	H_3	# of events
1	.360	3.795	.997	4.956	2.53×10^6
2	.605	3.819	1.005	5.006	1.84×10^6
3	2.970	1.958	1.010	5.200	3.35×10^6

Table IV. Independence of statistics with focal length.

v = .605 cm/sec. $\Psi = 0$

Exp. #	f (cm)	$\langle n \rangle$	H_2	H_3	# of events
1	19.39	3.819	1.005	5.006	1.84×10^6
2	27.00	3.700	.990	5.022	3.65×10^6
3	15.78	3.884	.976	4.817	3.37×10^6
4	10.30	3.834	1.019	5.186	3.56×10^6

Table V. Independence of statistics with angle.

f = 19.39 cm v = .605 cm/sec.

Exp #	ψ (degrees)	$\langle n \rangle$	H_2	H_3	# of events
1	0.0	4.350	.989	5.000	3.40×10^6
2	11.5	1.340	.994	4.967	2.7×10^6
3	21.0	.1754	1.022	5.115	5.88×10^6

Figure 11

Experimental distribution, 1 μ ground glass. The points represent the experimental data while the straight line is a theoretical Bose distribution with the same mean number

linear velocity	v	=	.605 cm.sec.$^{-1}$
focal length	f	=	19.44 cm.
scattering angle	ψ	=	0°
counting interval		=	25 μsec.
Off time		=	100 μsec.
Number of events		=	1.84 x 10^{6}

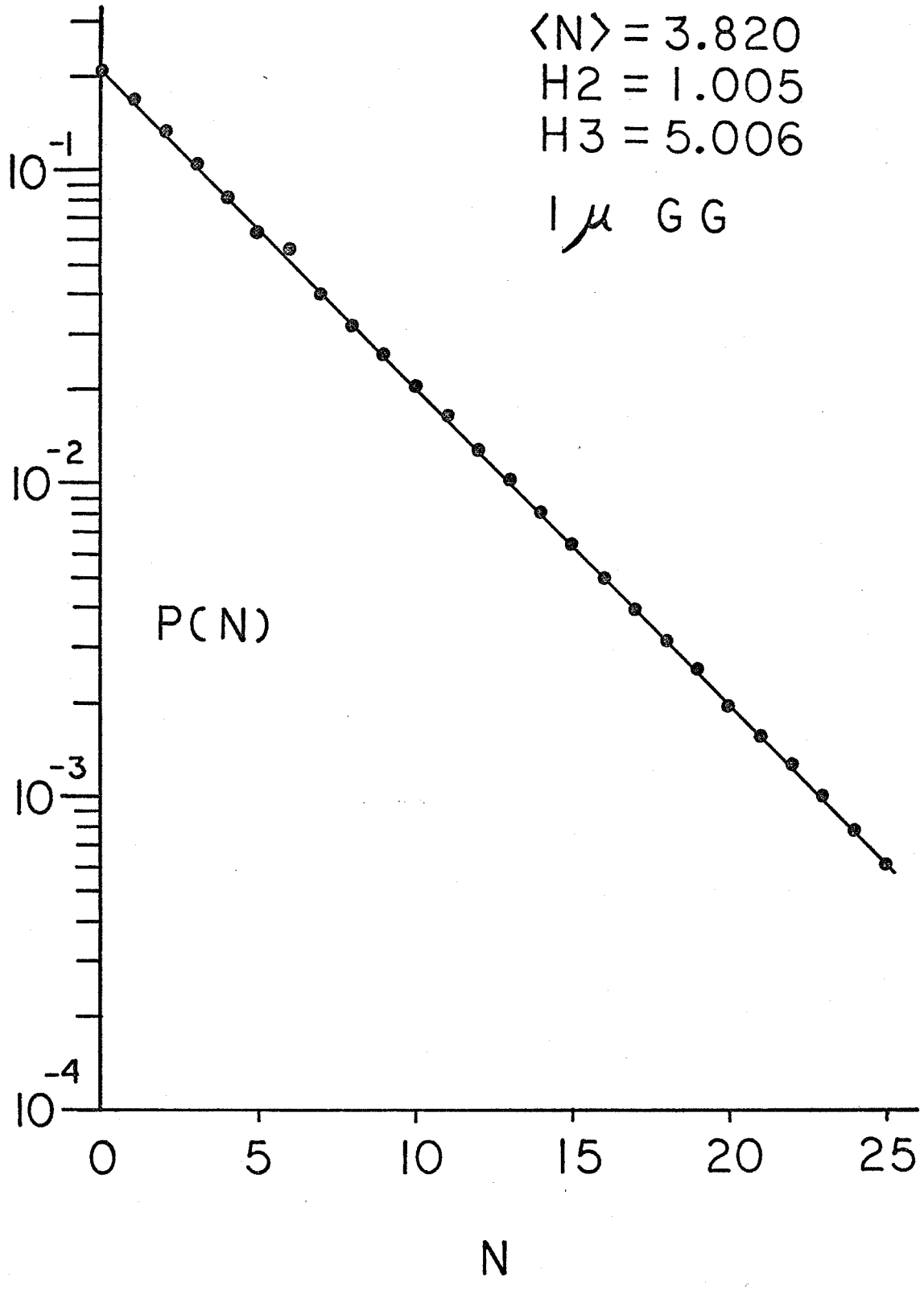
⟨N⟩ = 3.820
H2 = 1.005
H3 = 5.006
1 μ GG
P(N)
10^-1
10^-2
10^-3
10^-4
0
5
10
15
20
25
N

Figure 12

Experimental distribution, 1 μ ground glass.

v = .605 cm.sec.$^{-1}$

f = 19.44 cm.

ψ = 11.5°

Counting interval = 25 μsec.

Off time = 100 μsec.

Number of events = 2.78 x 10^{6}

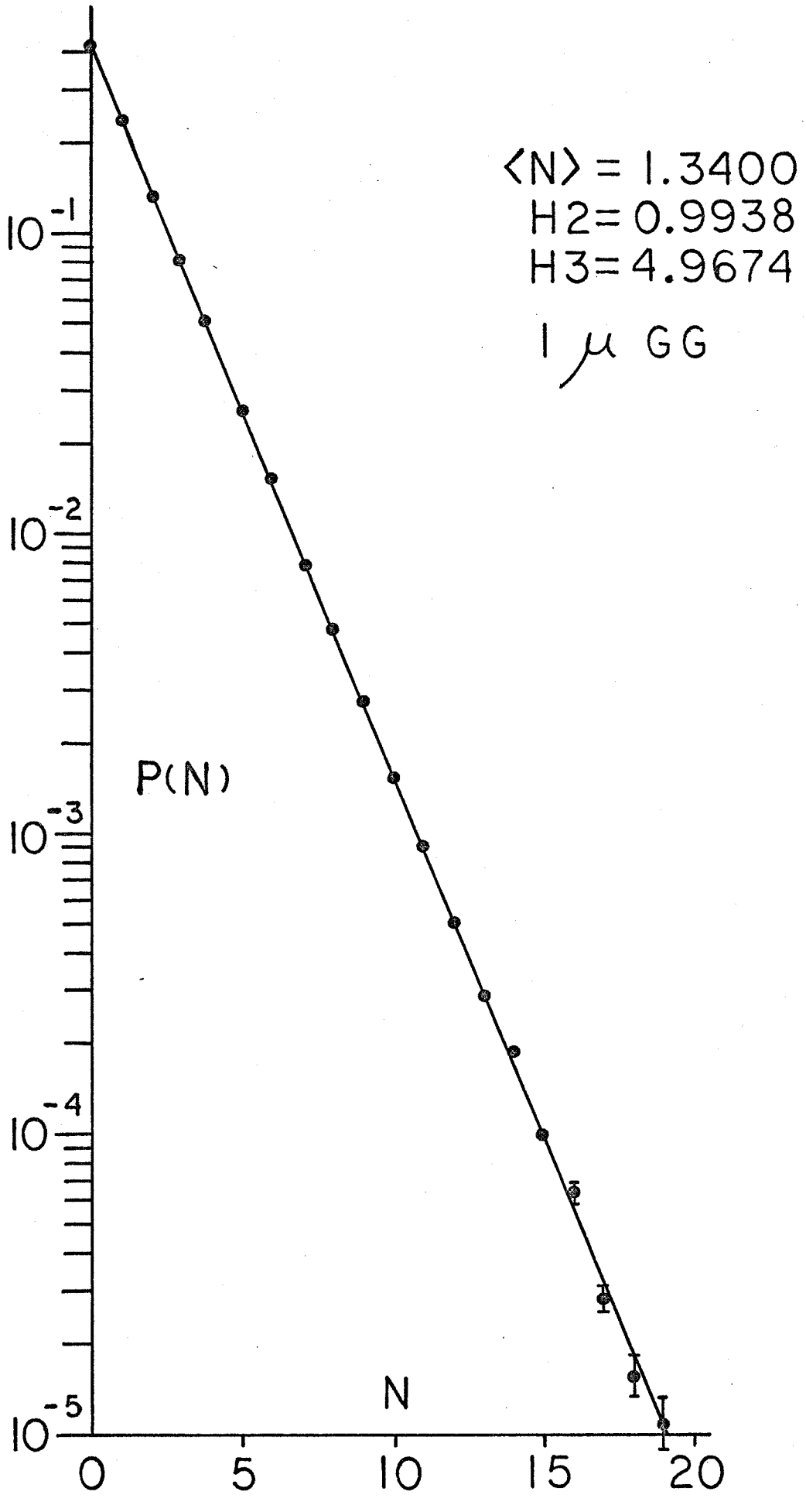
⟨N⟩ = 1.3400
H2 = 0.9938
H3 = 4.9674
1 μ GG
P(N)
N
10^-1
10^-2
10^-3
10^-4
10^-5
0
5
10
15
20

E. The Coarse Ground Glass, Discussion

The previous discussion was confined to a ground glass with average irregularities on the order of 1 micron. There were, therefore, many scatterers within the twenty to sixty micron diameter illuminated area on the ground glass. Thus the classical arguments for Gaussian field statistics which were advanced in Section III.B are expected to be valid.

An interesting situation, not previously investigated, is obtained when the size of the irregularities on the ground glass become comparable in size to the size of the illuminated region. In this case, we have no concise a priori derivation of the field amplitude probability distribution. An analogy with the case of electro-magnetic transmission through a turbulent atmosphere suggests that, since in this case the conditions of the Rytov approximation[30] are met, the distribution might be log-amplitude normal. That is, if A represents the field amplitude, then

$$P\left[\ln\left(A/A_0\right)\right] = \frac{e^{-\frac{\left[\ln\left(A/A_0\right)\right]^2}{2\sigma^2}}}{\sqrt{2\pi}\,\sigma} \quad . \qquad \text{(III.34)}$$

The transformation of this probability density to one for intensity and its substitution into the Mandel formula (Eq. III.1) has been done by Dr. George Riley.[31] The result is

$$P(n,T) = \int_0^\infty \frac{(\alpha I)^n e^{-\alpha I}}{n!} \left[\frac{1}{2I} \frac{e^{-\frac{(\ln I/I_0)^2}{8\sigma^2}}}{\sqrt{2\pi}\,\sigma} \right] dI . \quad \text{(III.35)}$$

This integral is untractable analytically, and one must resort to approximations or to numerical integration to get at P(n,T). Discussion on this point will be deferred for a time, however, since it is possible to obtain some relationships between the moments of the distribution P(n,T).

For the case in which the photoelectron counting is done within a coherence time, the factorial moments of the counting distribution are simply related to moments of the intensity distribution. Specifically, the factorial moment F_m is given by:[32]

$$F_m = \left\langle \frac{n!}{(n-m)!} \right\rangle = \sum_{n=0}^{\infty} n(n-1)\cdots(n-m+1)\, P(n,T)$$

$$= \left\langle (\alpha I)^m \right\rangle = \alpha^m \int_0^\infty I^m P(I)\, dI . \quad \text{(III.36)}$$

In particular, the reduced factorial moments are:

$$H_m = \frac{F_m - F_1^m}{F_1^m} = \frac{\langle I^m \rangle - \langle I \rangle^m}{\langle I \rangle^m} \qquad \text{(III.37)}$$

and the mean number is given by

$$F_1 = \langle n \rangle = \alpha \langle I \rangle . \qquad \text{(III.38)}$$

Now

$$\langle I^m \rangle = \int_0^\infty I^m \frac{1}{2I} \frac{e}{\sqrt{2\pi}\sigma} e^{-\frac{(\ln I - \ln I_0)^2}{8\sigma^2}} dI . \qquad \text{(III.39)}$$

We let

$$y = \ln I \quad , \quad y_0 = \ln I_0 ,$$

$$dI = e^y dy .$$

Then Eq. III.39 becomes

$$\langle I^m \rangle = \int_{-\infty}^{\infty} \frac{e^{my}}{2\sqrt{2\pi}\sigma} e^{-\frac{(y-y_0)^2}{8\sigma^2}} dy . \qquad \text{(III.40)}$$

Using $y - y_o = z$,

$$\langle I^m \rangle = \frac{e^{my_o}}{2\sqrt{2\pi}\sigma} \int_{-\infty}^{\infty} e^{mz}\, e^{-z^2/8\sigma^2}\, dz \quad . \qquad \text{(III.41)}$$

This integral is of the form[33]

$$\int_{-\infty}^{\infty} e^{ax^2+bx}\, dx = \sqrt{\frac{\pi}{-a}}\; e^{-b^2/4a} .$$

So we have

$$\langle I^n \rangle = \frac{e^{my_o}}{\sqrt{8\pi\sigma^2}}\, \sqrt{8\pi\sigma^2}\; e^{2m^2\sigma^2}$$

or

$$\langle I^m \rangle = I_o^m\, e^{2m^2\sigma^2} . \qquad \text{(III.42)}$$

Thus, from Eq. III.38

$$\langle n \rangle = \alpha I_o\, e^{2\sigma^2} , \qquad \text{(III.43)}$$

and from Eq. III.37

$$H_m = \frac{\langle I^m \rangle - \langle I \rangle^m}{\langle I \rangle^m} = \frac{I_o^m\, e^{2m^2\sigma^2} - I_o^m\, e^{2m\sigma^2}}{I_o^m\, e^{2m\sigma^2}}$$

or

$$H_m = e^{2\sigma^2(m^2-m)} - 1 . \qquad \text{(III.44)}$$

In particular,

$$H_1 = 0$$

$$H_2 = e^{4\sigma^2} - 1 \qquad \text{(III.45)}$$

$$H_3 = e^{12\sigma^2} - 1 \quad .$$

So we have the relation between H_2 and H_3,

$$H_3 = (H_2 + 1)^3 - 1 \quad , \qquad \text{(III.46)}$$

which will be useful in characterizing the experimental distributions.

The integration of Eq. III.35, as has already been noted, has not yet been accomplished in a closed form. Several methods of obtaining $P(n,T)$ have been attempted. These include the method of steepest descent[34] and a numerical integration.[35] The method of steepest descent solution appears to violate some of the criteria[36] for the validity of the method in the range of the relevant parameters of the distribution which occurred within our experiments. Indeed, for the low mean numbers

occurring in Dr. Riley's experimental work, the method of steepest descent formula did not provide a normalized distribution.[37]

The numerical integration, while accurate, consumes large amounts of computer time. To circumvent this difficulty, a computer program was written which calculated $P(0,T)$ by a Simpson's rule integration[38] and all higher probabilities by means of a Gauss-Laguerre quadrature.[38] In this technique, an approximation is made to an integral of the form

$$\int_0^\infty e^{-x} f(x)\, dx = \sum_{j=1}^{n} H_j f(a_j) .$$

Here the a_j's are roots of an nth order Laguerre polynomial $L_n(x)$, and

$$H_j = \frac{(n!)^2}{a_j \left[\frac{d}{dx} L_n(x) \Big|_{a_j} \right]^2} .$$

The $\{a_j\text{'s}\}$ and $\{H_j\text{'s}\}$ are tabulated up to $n = 15$ in several places.[39]

The integration of P(0,T) was done by Simpson's rule because errors in the computation at points near the origin gave rise to large errors in a Gauss-Laguerre integration for this case. Because the Gauss-Laguerre integration is much faster than a Simpson's rule integration, the program could be written in FOCAL for the relatively slow PDP-8/L computer. A program listing is given in Appendix B. The program computes σ^2 from Eq. III.45 using the value of H_2 for a given experimental distribution. Using this value of σ^2, the quantity αI_0 can be determined from the experimental value of $\langle n \rangle$ using Eq. III.43. These two parameters are sufficient to determine the log-normal distribution uniquely.

A comparison between the results of the FOCAL program and those of the numerical integration (or NUMINT) program written by Dr. Riley is given in Appendix C. The agreement is quite good and provides some justification for the use of the much faster Gauss-Laguerre integration in preference to the slower numerical integration. The inclusion of expected errors due to finite counting statistics was accomplished in the same manner as it was for the Bose-Einstein distribution.

F. Experimental Results, 20 micron Ground Glass

To investigate the hypothesis that the photo-count distribution of the scattered light might be characterized by a log-amplitude normal distribution when the size of the ground glass irregularities become comparable to the size of the illuminated region, a coarse ground glass was prepared.

A nine-inch diameter by one-quarter inch thick piece of plate glass was hand ground using another piece of plate glass as a tool. The grit used was number 220 silicon carbide abrasive.[40] By carefully replenishing the abrasive at frequent intervals during the grinding, so that the grit size was not reduced appreciably, the final large scale irregularities on the ground glass were maintained in the range of 20 to 60 microns. There were also many small scale irregularities on the order of a few microns.

The far field diffraction pattern of this ground glass was markedly different from the one exhibited by the 1 micron ground glass used in the previous experiments. It was characterized by very large illuminated areas widely separated. When the glass was set in motion, the pattern

exhibited occasional high intensity flashes that were never present for the 1 micron glass.

Experimental counting distributions for several values of v, f and ψ are given in Figures 13 through 17 together with a theoretical Bose distribution with the same mean number and a log-amplitude normal distribution with the same mean number and H_2. In most cases the agreement is quite good, especially since no attempt was made to fit the shape of the experimental distribution. Only the first two moments of the experimental distribution were used to generate the theoretical distribution. Since the second moment is somewhat sensitive to counting errors for the higher count numbers, we can expect some discrepancy in the tail of the distribution.

The best fit to a log-amplitude normal distribution appears to occur at short focal lengths (3.8 and 10.15 cm) and large scattering angles. For small scattering angles and long focal lengths, the experimental distribution falls off more rapidly with n than does the theoretical log-amplitude normal distribution. This is probably due to an increase in the contribution to the fluctuations of the small scale irregularities previously noted. This

Figure 13

Experimental distribution, 20 μ ground glass
The points represent the data.
The solid curve marked L - N represents a computer generated log-normal distribution determined from the experimental values of $\langle N \rangle$ and H2..
The line marked B - E is a Bose-Einstein distribution with the experimental $\langle N \rangle$.
v = 1.329 cm.sec.$^{-1}$
f = 3.8 cm.
ψ = 16.4°
Counting interval = 25 μsec.
Off time = 100 μsec.
Number of events = 9.35 x 10^{6}

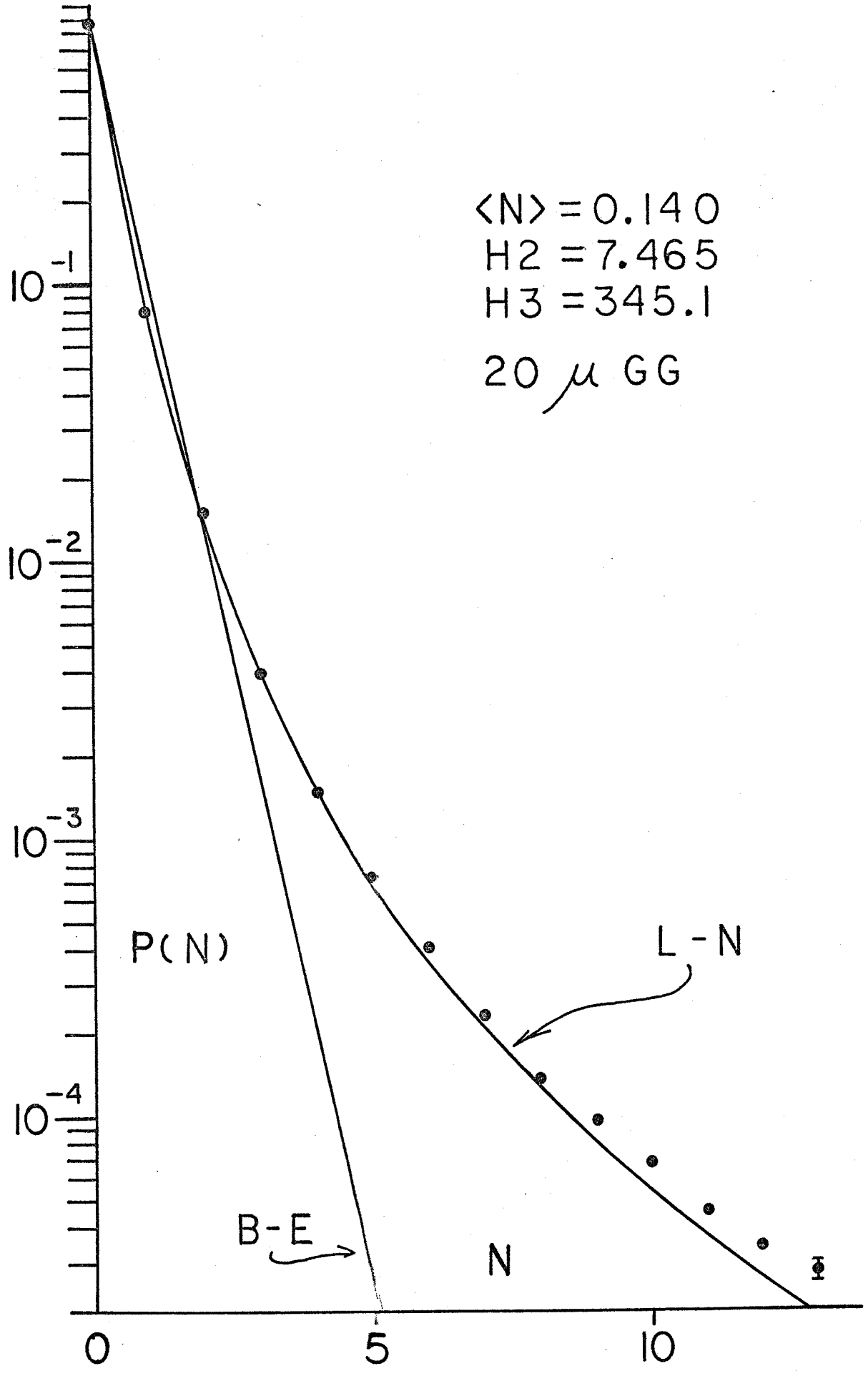
⟨N⟩ = 0.140
H2 = 7.465
H3 = 345.1
20 μ GG
10^-1
10^-2
10^-3
10^-4
P(N)
L-N
B-E
N
0
5
10

Figure 14

Experimental distribution, 30 μ ground glass.

Data: points

Log-normal using $\langle N \rangle$ and σ^2: L - N

Bose-Einstein using $\langle N \rangle$: B - E

$v = 2.970$ cm. sec.$^{-1}$

$f = 10.15$ cm.

$\psi = 16.4^{\circ}$

Counting interval = 25 μsec.

Off time = 100 μsec.

Number of events = 9.32×10^6

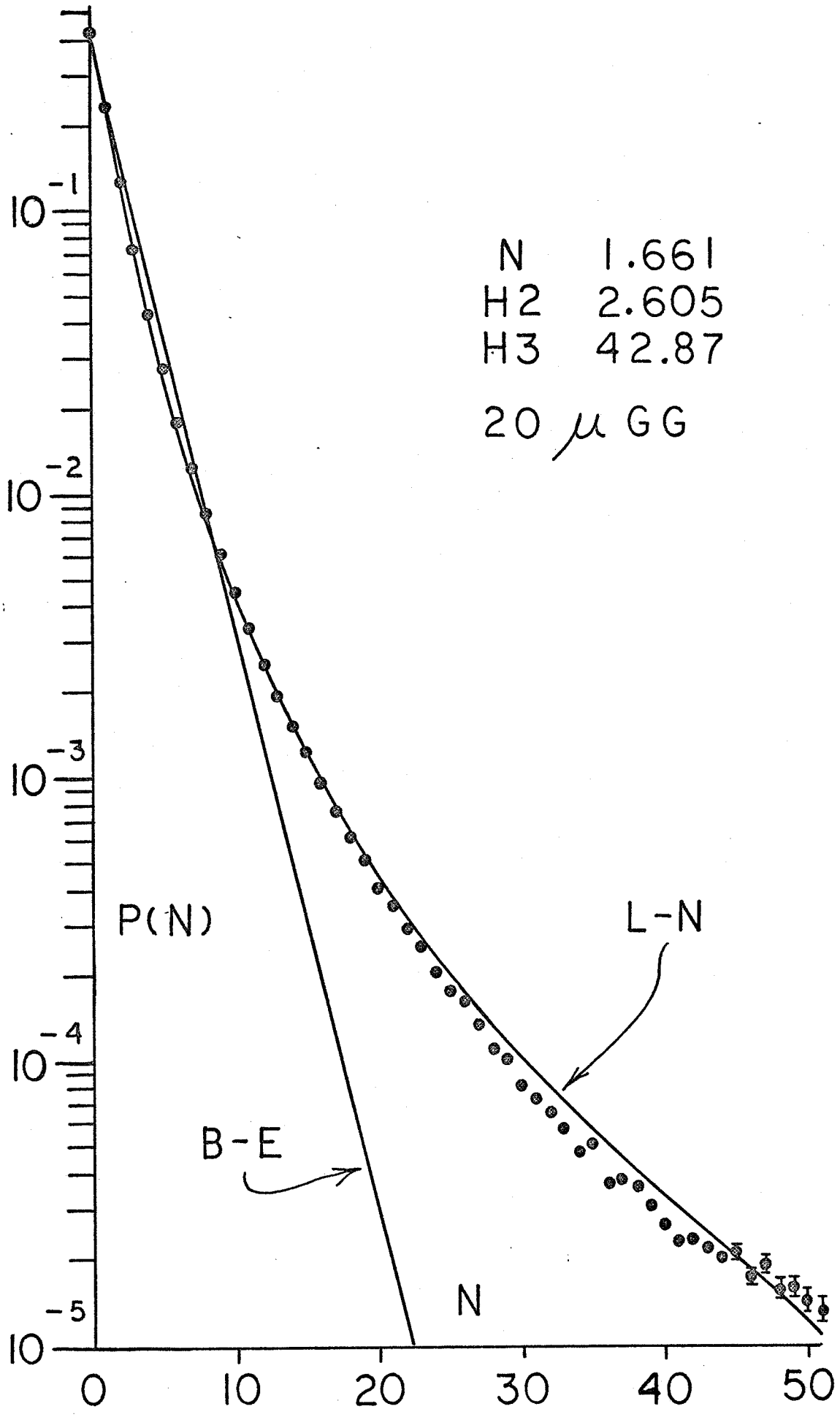
N 1.661
H2 2.605
H3 42.87
20 μ GG
P(N)
L-N
B-E
N
10^-1
10^-2
10^-3
10^-4
10^-5
0
10
20
30
40
50

Figure 15

Experimental distribution, 20 μ ground glass

Data: points

Log-normal using $\langle N \rangle$ and H2: L - N

Bose-Einstein using $\langle N \rangle$: B - E

$v = 1.329$ cm. $sec.^{-1}$

$f = 10.15$ cm.

$\psi = 0^{\circ}$

Counting interval = 25 μsec.

Off time = 100 μsec.

Number of events = 7.65×10^{6}

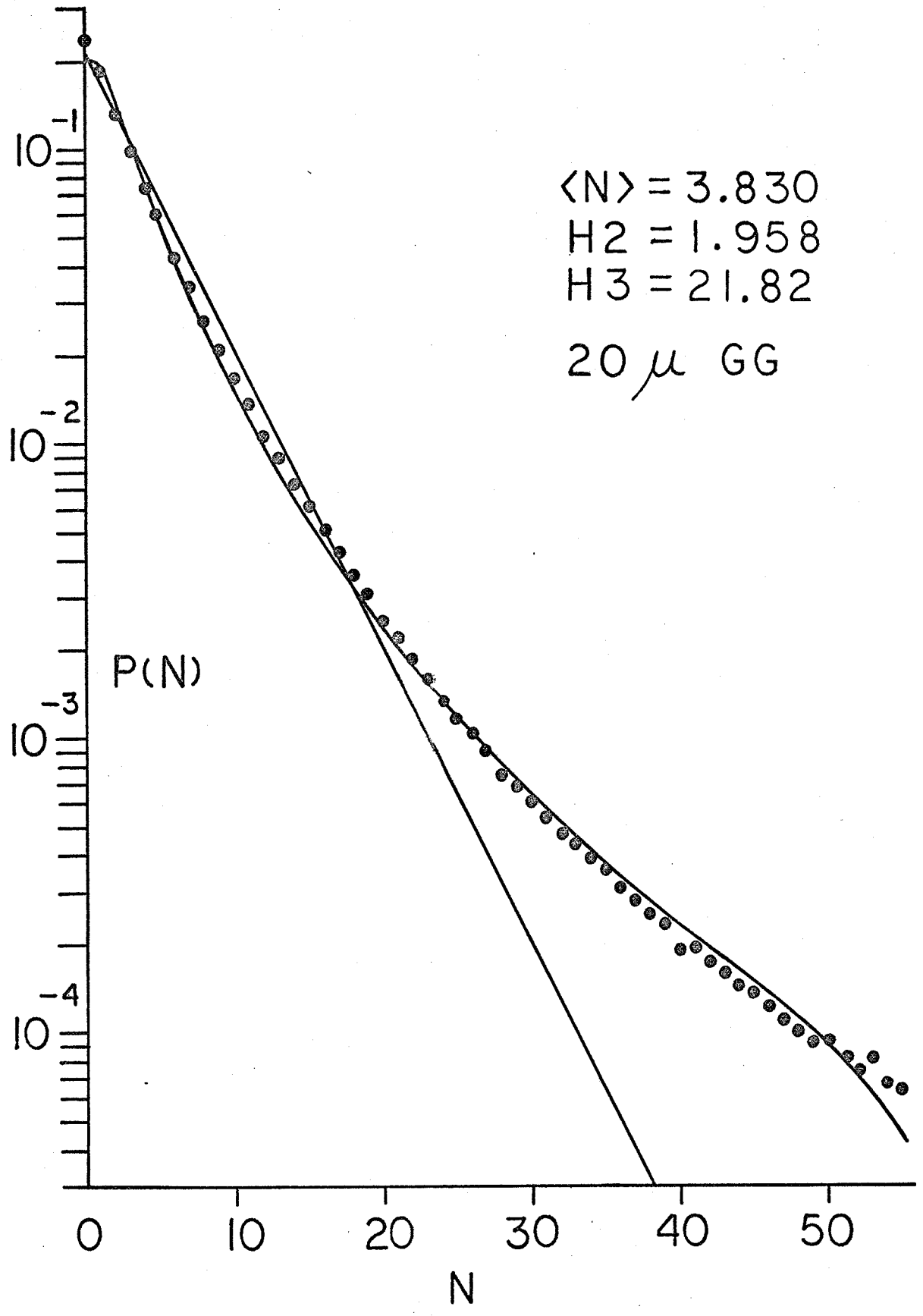
⟨N⟩ = 3.830
H2 = 1.958
H3 = 21.82
20 μ GG
P(N)
10^-1
10^-2
10^-3
10^-4
0
10
20
30
40
50
N

Figure 16

Experimental distribution, 30 μ ground glass.

Data: points.

Log-normal using $\langle N \rangle$ and H2: L - N

Bose-Einstein using $\langle N \rangle$: B-E

$v = 1.329$ cm.sec.$^{-1}$

$f = 19.44$ cm.

$\psi = 0^{\circ}$

Counting interval = 25 μsec.

Off time = 100 μsec.

Number of events = 8.26×10^{6}

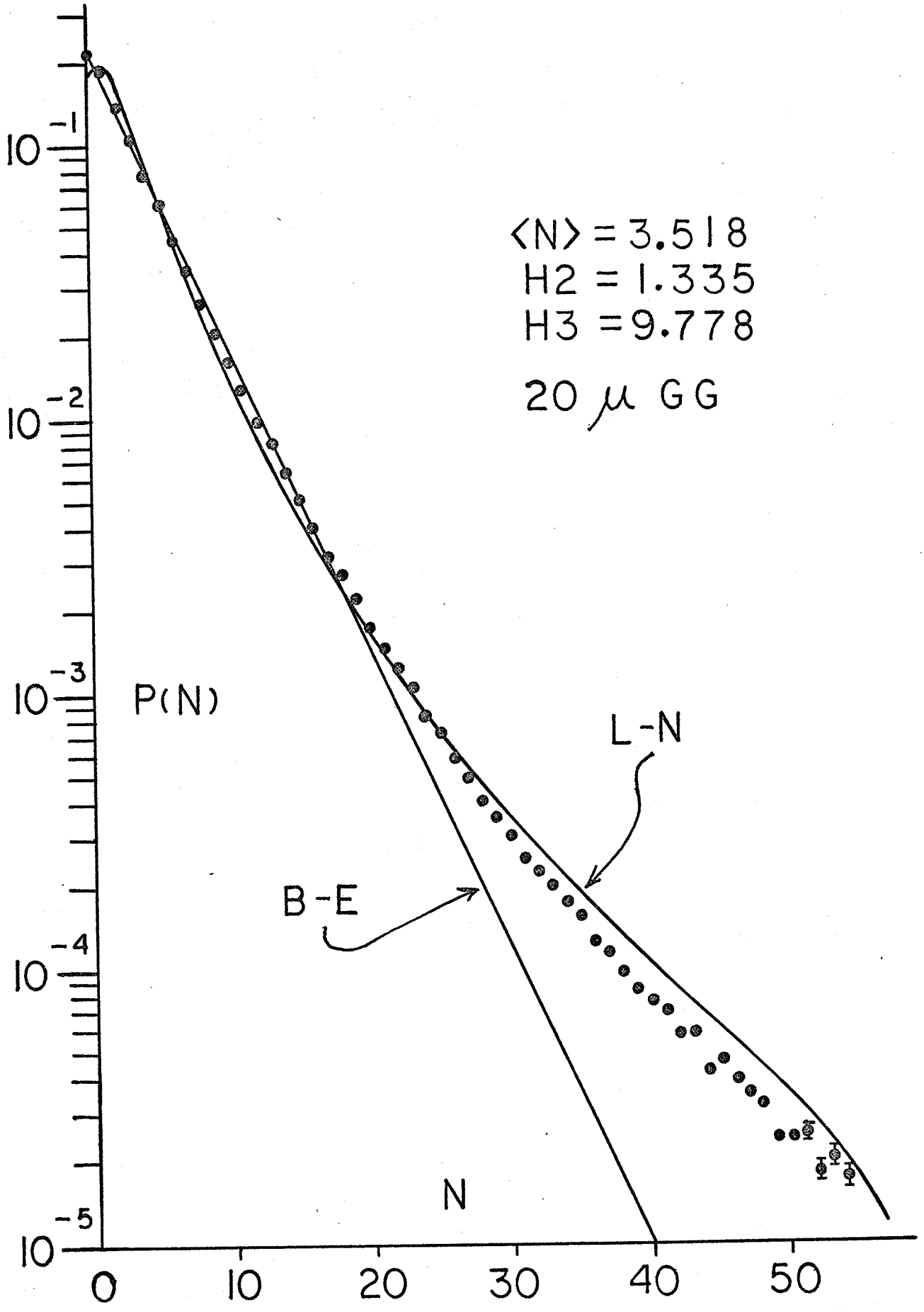
⟨N⟩ = 3.518
H2 = 1.335
H3 = 9.778
20 μ GG
P(N)
L-N
B-E
N
10^-1
10^-2
10^-3
10^-4
10^-5
0
10
20
30
40
50

Figure 17

Experimental distribution, 20 μ ground glass

Data: points

Log-normal using $\langle N \rangle$ and H2: L-N

Bose-Einstein using $\langle N \rangle$: B-E

$v = 1.329$ cm.sec.$^{-1}$

$f = 30.54$ cm.

$\psi = 16.4^{\circ}$

Counting interval = 25 μsec.

Off time = 100 μsec.

Number of events = 14.9×10^{6}

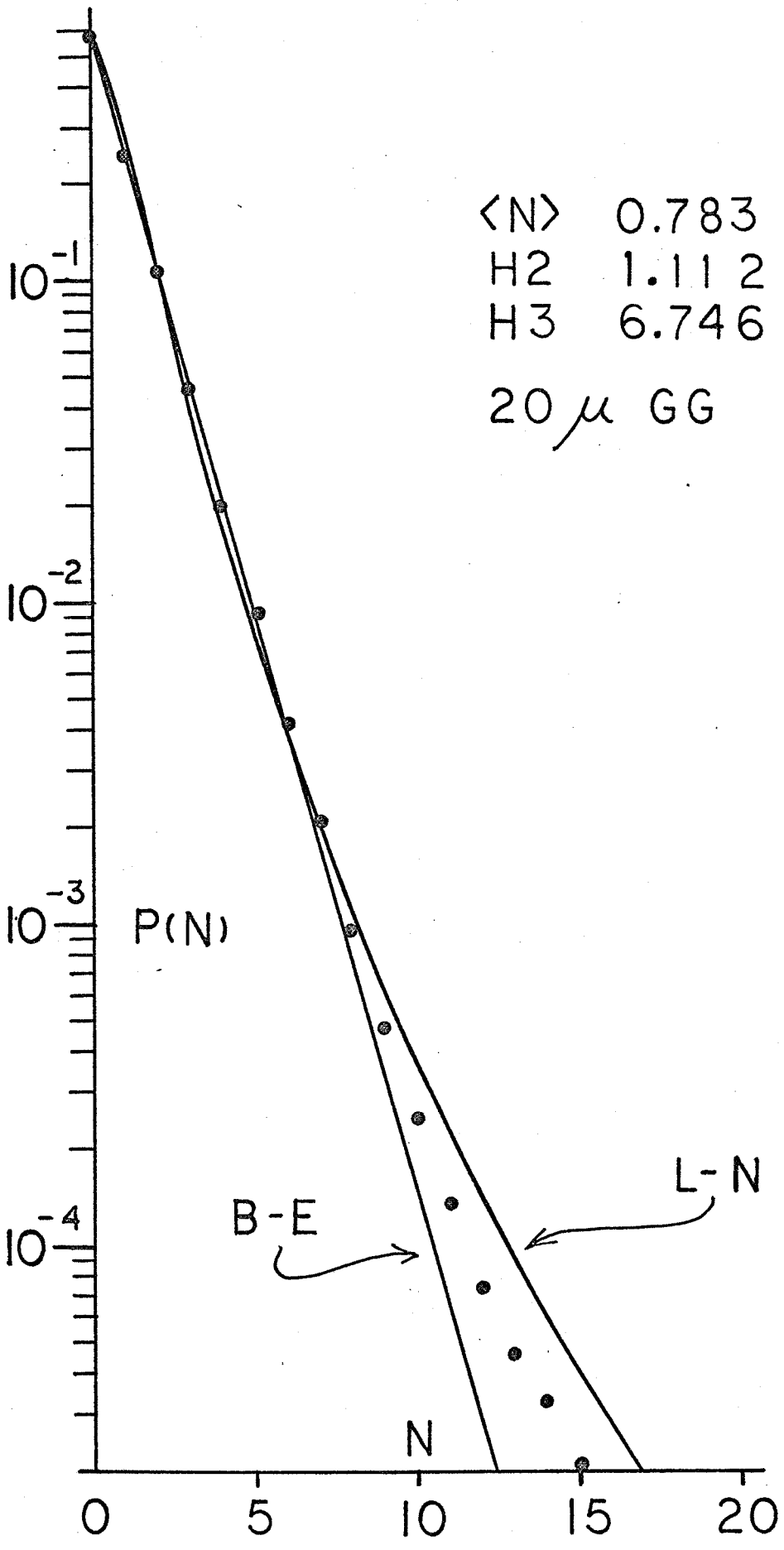
⟨N⟩ 0.783
H2 1.112
H3 6.746
20 μ GG
10^-1
10^-2
10^-3
10^-4
P(N)
B-E
L-N
N
0
5
10
15
20

supposition led to the further conjecture that the contribution of the small scale granularity might result in a superposition of Bose-Einstein and log-amplitude normal distributions.

To test this hypothesis, the data of Figure 17 was subjected to a test to see if it could possibly be such a superposition. For this purpose, the set of Eqs. III.29 were used to obtain three equations in the three unknowns $\langle n^{BE} \rangle$, $\langle n^{LN} \rangle$, and H_2^{LN} (the mean number of the Bose-Einstein contribution and the mean number and H_2 of the log normal contribution respectively). These equations are:

$$\langle n^E \rangle = \langle n^{BE} \rangle + \langle n^{LN} \rangle$$

$$\langle n^E \rangle^2 H_2^E = \langle n^{BE} \rangle^2 H_2^{BE} + \langle n^{LN} \rangle^2 H_2^{LN} \qquad \text{(III.47)}$$

$$\langle n^E \rangle^3 (H_3^E - 3 H_2^E) = \langle n^{BE} \rangle^3 (H_3^{BE} - 3 H_2^{BE}) + \langle n^{LN} \rangle^3 (H_3^{LN} - 3 H_2^{LN}) .$$

In Eqs. III.47, we know that $H_2^{BE} = 1.000$, $H_3^{BE} = 5.000$ and, from Eq. III.46, $H_3^{LN} = (1 + H_2^{LN})^3 - 1$.

The set of simultaneous equations III.47 were solved on the PDP-8/L computer using an iterative technique. A trial value of $\langle n^{BE} \rangle$ was selected and the first and second equations were used to compute $\langle n^{LN} \rangle$ and H_2^{LN} . The third equation was then checked for consistency by subtracting the right-hand side from the left-hand side and minimizing this value.

No roots to this set of equations were found in the region of physical possibility; that is, no roots were found for

$$0 \leq \langle n^{BE} \rangle \leq \langle n^{E} \rangle \ .$$

It can only be concluded that the original hypothesis was wrong and that, in fact, the distribution cannot be a superposition of independent Bose-Einstein and log-amplitude normal distributions.

IV. CONCLUSION

The results presented herein complete and extend a number of previous investigations[2,41] conducted to study the statistical properties of a coherent beam of light scattered by a rotating ground glass.

Measurements on the scattering of light from a ground glass of one micron average size inhomogeneities have verified that the statistical distribution of the photoelectrons ejected from the surface of the detecting device by the scattered beam is Bose-Einstein. The power spectral broadening due to the motion of the ground glass through the incident beam has been predicted and verified to be a Gaussian function of the frequency.

For the case of a ground glass with inhomogeneities on the order of twenty microns, a significant departure from Bose-Einstein photocount statistics is observed. This indicates that the field amplitude probability distribution can no longer be Gaussian.

In the case that the illuminated area on the ground glass is on the order of the size of the inhomogeneities, it is found that the assumption of a log-amplitude normal field probability distribution provides a very good fit to the photocount data.

A shortened account of the results of this thesis will be published in a future issue of the Journal of the Optical Society of America.[42]

APPENDIX A

THE PHOTON COUNTING SYSTEM

CONTENTS

FIGURES

1. Description of the System

The photocount system uses a PDP-8/L computer as a 512 channel analyzer. A block diagram of the system is given in Figure A1. A brief description of the system follows.

The output of the photomultiplier tube (PMT) is amplified by a factor of 100 using the Lecroy 134 wideband amplifier. The output of the amplifier goes to one channel of a Lecroy 520A 200 MHz dual scaler. This scaler counts the number of photoelectron pulses emitted by the photomultiplier during a counting interval determined by the output pulse width of the Advanced Automation 2000 generator.

At the end of a counting interval the Hewlett Packard 222A generator sends a pulse to the interface, which initiates read in of the number of counts in the scaler into the computer. After the data have been read in, a pulse is sent from the interface to start another counting interval. The computer, at the same time, begins execution of a program which will increase by one the number stored in the channel corresponding to the number of counts just read in. The data gathering proceeds in this manner.

Figure A1

Photocount system block diagram.

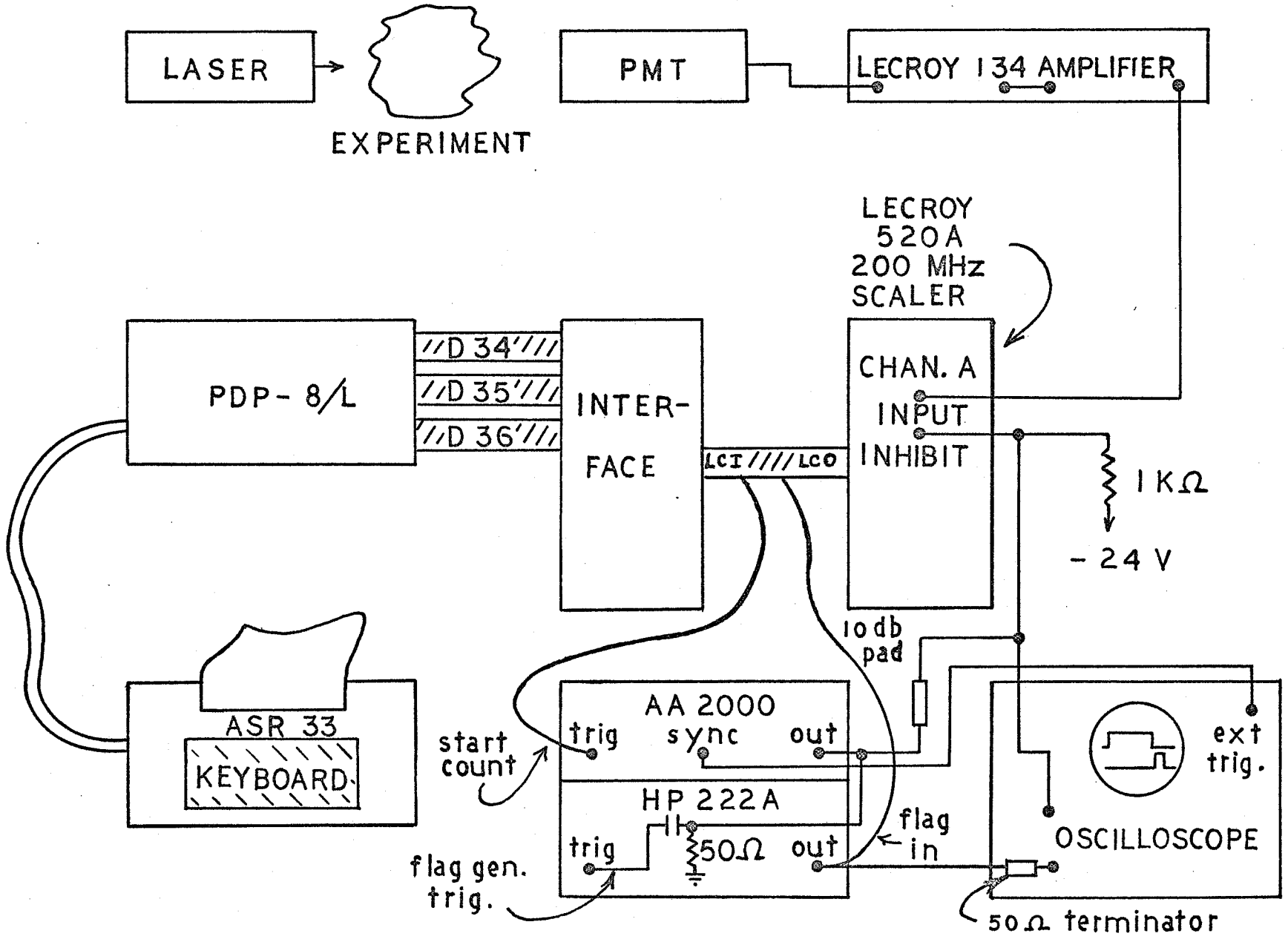
LASER
EXPERIMENT
PMT
LECROY 134 AMPLIFIER
LECROY
520A
200 MHz
SCALER
PDP-8/L
//D 34'///
//D 35'///
//D 36'///
INTER-
FACE
LCI////LCO
CHAN. A
INPUT
INHIBIT
1KΩ
-24 V
10 db
pad
ASR 33
KEYBOARD
start
count
AA 2000
trig
sync
out
HP 222A
trig
50Ω
out
flag
in
flag gen.
trig.
ext
trig.
OSCILLOSCOPE
50Ω terminator

Data is accumulated until either the channel corresponding to the most probable number of counts overflows (channel capacity is approximately 8.4×10^6 events) or the experiment is terminated by the operator from the teletype keyboard.

The computer then calculates the probabilities, P(n), for the number of counts in a counting interval. It also prints out the first and second moments of the probability distribution, $\langle n \rangle$ and $\langle n^2 \rangle$, as well as the reduced factorial moments;

$$H_2 = \frac{\langle n^2 \rangle - \langle n \rangle - \langle n \rangle^2}{\langle n \rangle^2}$$

$$H_3 = \frac{\langle n^3 \rangle - 3\langle n^2 \rangle + 2\langle n \rangle - \langle n \rangle^3}{\langle n \rangle^3} \quad .$$

All calculations are to six significant figures. The printout also includes the number of events (i.e., the number of counting intervals) occurring in the course of the experiment.

The requirement that the counting interval be much less than the relaxation time of the scatterer under study may be easily met by setting the pulse width

of the Advanced Automation generator. The requirement that the counting intervals be separated by a time greater than the relaxation time of the scattering mechanism can be met by delaying the output of the Advanced Automation generator with respect to the start pulse sent by the interface. Such a variable delay is a feature of the generator.

2. Some Notes on the PDP-8/L

It is recommended that before trying to run the system, whose operation is primarily dependent upon the computer, some attempt be made to familiarize oneself with the computer controls. It would seem that a reading of the first 23 pages of the DEC Small Computer Handbook is a minimum in this regard.

For a more detailed knowledge of the system, and as a prerequisite for understanding and troubleshooting the interface, chapters 9, 11 and 12 of the same manual are recommended reading.

As a reminder, and to keep easily forgotten facts at hand, the following computer information is presented.

The Computer Number System

The PDP-8/L computer is a 12 bit machine. That is, it does arithmetic on binary numbers with 12 binary digits or bits, a bit being either 0 or 1. The bits are numbered from left to right and have the following position coefficients:

Bit No.	0	1	2	3	4	5	6	7	8	9	10	11
Value	2^{11}	2^{10}	2^{9}	2^{8}	2^{7}	2^{6}	2^{5}	2^{4}	2^{3}	2^{2}	2^{1}	2^{0}

Thus the binary number

100100111

can be found in decimal as:

$$
\begin{aligned}
1 \times 2^{0} &= 1 \times 1 = 1 \\
1 \times 2^{1} &= 1 \times 2 = 2 \\
1 \times 2^{2} &= 1 \times 4 = 4 \\
0 \times 2^{3} &= 0 \times 8 = 0 \\
0 \times 2^{4} &= 0 \times 16 = 0 \\
1 \times 2^{5} &= 1 \times 32 = 32 \\
0 \times 2^{6} &= 0 \times 64 = 0 \\
0 \times 2^{7} &= 0 \times 128 = 0 \\
1 \times 2^{8} &= 1 \times 256 = 256 \\
&\qquad\qquad\quad 295
\end{aligned}
$$

It should be apparent that 12 bit binary numbers are rather cumbersome, so the computer is set up to recognize commands as 4 character octal numbers. These octal numbers are really the 12 bit binary numbers handled in a slightly different manner. They are formed by beginning with a binary number, say

011010111101

and separating it into 3 bit groups starting at the right:

011 010 111 101.

The binary groups are then replaced by their octal equivalents:

$$011_2 = 3_8$$

$$010_2 = 2_8$$

$$111_2 = 7_8$$

$$101_2 = 5_8$$

and the binary number is converted to its octal equivalent:

3275.

Conversely, an octal number can be expanded to a binary number using the same table of equivalents:

$$5307_8 = 101\ 011\ 000\ 111_2$$

3. The PDP-8/L Front Panel

In order to run the photocount system, it is necessary to be able to manipulate the front panel controls of the PDP-8/L. The use of the front panel in the operations necessary to load and run the system software is summarized below. For more detailed information, check the DEC Small Computer Handbook, Ch. 2.

1. Loading Program Tapes.
   a) MEM PROT, DATA FIELD, INST FIELD: all down. SING STEP: up.
   b) Bits 0 thru 11 of the SWITCH REGISTER: all up (7777 octal).
   c) Depress LOAD ADDR momentarily. All lights under MEMORY ADDRESS should light up.
   d) Turn teletype control to LINE. Set reader switch to FREE. Load paper tape into reader.
   e) Turn reader switch to START.
   f) Depress START on front panel. Tape should read in.
2. Loading Addresses and Checking Contents.
   a) Set the address into the SWITCH REGISTER in octal. A switch up is a binary one, down a zero.

b) Depress LOAD ADDR. Check MEMORY ADDRESS lights for correct address.

c) Check MEMORY BUFFER lights for octal contents of address.

d) Repeated pressing of the EXAMINE switch will increment the addresses one by one, allowing you to examine the contents of successive locations.

3. Changing the Contents of an Address

a) Follow steps 2a) through 2c) above.

b) Set the desired octal content of the address into the SWITCH REGISTER.

c) Raise up the DEP switch. This deposits the contents of the SWITCH REGISTER in the selected address.

d) Contents of the succeeding locations can be altered by setting the desired contents into the SWITCH REGISTER in sequence and raising the DEP switch after each setting of the SWITCH REGISTER.

4. Running the System

1. If the Multichannel Analyzer program is in core, begin at step 5. If not, load address 7777 by means of the SWITCH REGISTER of the PDP-8/L.

2. Load the MCA tape into the paper tape reader, make sure the teletype is on LINE, and turn on the reader.
3. Press START. Tape should read in and stop at roughly one-third of the way through.
4. When the tape stops, press CONT. This loads the Floating Point Arithmetic package. Entire MCA program is loaded when tape stops.
5. Select Options:
   a) Address 0020 normally contains 1000. The program will normally print out 1000 octal channels (512 decimal). If fewer channels are desired, the desired octal number may be inserted in location 20.
   b) Address 0021 normally contains a 0. This allows the program to skip an automatic octal dump of the number of events in each channel after the printout of probabilities. If automatic octal dump is desired, any number $\neq 0$ may be put in this address.
   c) Address 0022 normally contains a 1. This sends the program into a waiting routine after either the printout of probabilities or octal dump. If set = 0, will halt the program instead of waiting.

6. Begin setup of the system.

   a) Turn on interface and rest of experiment.

   b) System interconnections should be as shown in Figure A1. The generator settings should be:

      i) HP 222A

         Rep Rate : EXT. -

         Pulse Delay : .1 to .5 μsec or desired value

         Pulse width : .5 μsec

         Pulse polarity: +

         Pulse amplitude: 2 volts

      ii) Advanced Automation 2000

         Rep Rate: EXT

         Gate: OFF

         NORMAL PULSE

         Delay: Desired Value

         Width: Desired Value

         Amplitude: + .5 volts

   c) Connect sync. output of Advanced Automation generator to external trigger input of oscilloscope. Set scope to trigger on positive signal.

   d) Using a 50 Ω terminator on one scope channel input, connect the output of the HP generator to the scope by means of a BNC tee. The "FLAG IN" cable must still go to the interface. Set scope channel gain to 2 v/cm DC. Use scope on alternate mode.

e) Using a BNC tee on the Lecroy channel A inhibit input, connect to other scope channel without a 50 Ω terminator. (Use of a 50 Ω terminator would load down the voltage divider that provides the negative bias to the inhibit.) Set scope channel gain to .5 v/cm.

f) By means of the SWITCH REGISTER, load address 0023. Press START. This initiates a setup program which continually supplies signals between the computer interface and the external generators. If no waveforms are displayed on the scope, press the STOP button on the front panel of the computer. Check the interconnections and generator settings (see 6b and 6c). Make sure interface power supply (+ 5 volts) is on. Reload address 0023 and press START again.

g) Set desired counting interval. This is done by setting the time that the Advanced Automation generator spends at 0 volts (0 volts lifts the inhibit, - .5 volts inhibits). The time between successive counting intervals may be varied by means of the pulse delay control on the Advanced

Automation generator. After setting counting interval and delay, check that the flag pulse (output of Hewlett Packard generator) follows the trailing edge of the counting interval. The trace on the oscilloscope should appear similar to below:

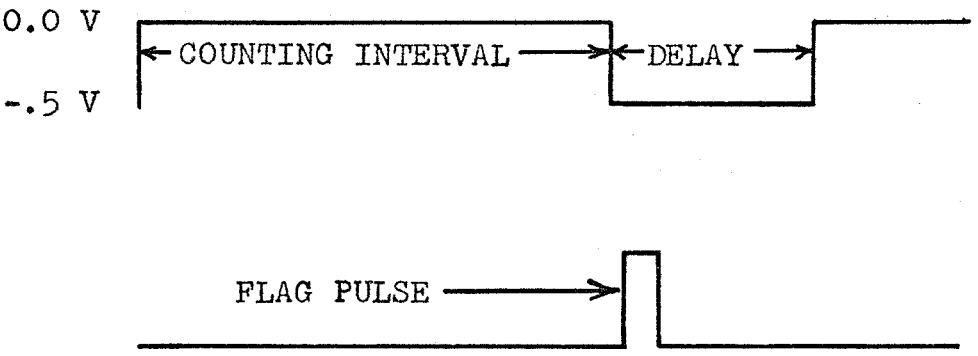

The minimum delay between counting intervals is roughly 12 to 18 microseconds owing to program delays. Additional delay between counting intervals, beyond that provided by the Advanced Automation generator, may be obtained by delaying the flag pulse using the delay control on the Hewlett Packard.

7. The main multichannel analyzer program is now started by loading address 5400 by means of the SWITCH REGISTER and pressing START. This begins the sequence of counting intervals. The counting will continue until

one channel overflows (at roughly 8 million events) or the counting is terminated from the teletype keyboard by pressing $.

8. When the counting stops, through either overflow or keyboard interruption using a $, the user then has several options available, depending upon the action taken in step 5. Roughly 8 seconds after the counting stops, the computer begins its printout routine. It will printout NBAR, N^2BAR, H2, H3, and the total number of events. It then begins printout of the probabilities for a given number of counts in a counting interval. It is at this point that the options become available.

   a) If left uninterrupted during the probability printout, the teletype will either printout all 1000 octal channels or the lower number inserted during step 5a). At the end of this printout, the teletype will type the sum of the probabilities which have been printed out. If, during probability printout a $ is pressed on the keyboard, the teletype will finish printing out the line it is on and will then print the sum of only the probabilities which have been printed out to that point.

b) What happens at this point depends on what was done in step 5b). If the octal dump was selected, it will begin immediately. This may be terminated at any time by a $ on the keyboard. If not terminated, the number of octal channels selected in 5a) will be printed out. Both channel number and channel content are given in octal numerical form. If octal dump was not selected, the program goes to the option described next.

c) After printout of the probabilities and the octal dump (if selected in step 5b), the program will either halt or go into a waiting routine depending upon the option selected in step 5c). If the program halts and it is desired to restart it, load address 5400 and press START. If it remains in the waiting routine, the following commands may be given from the keyboard:

C - continues count without clearing channels

R - restarts count after clearing channels

O - prints out octal dump

H - halts program

9. To shut down the system, press H when the computer is in the waiting routine, then turn off the computer and interface.

5. Description of Interface Logic and Timing

A logic diagram of the circuitry which accomplishes the transfer of data between the Lecroy 200 MHz scaler and the PDP-8/L computer is given in Figure A2. A more detailed breakdown to DEC Flipchip boards together with connector assignments may be found in Figure A4. A timing diagram to be used with Figure A2 is given in Figure A3. The description of interface timing following is done with reference to Figures A2 and A3.

The timing diagram begins with the computer in a routine which awaits the appearance of a flag (A), signifying the presence of data. Thus the Advanced Automation 2000 generator (I), which controls the time during which photoelectrons are counted, is still in the up state. The computer is initiating a series of 6141 IOT pulses (B) which, in the absence of a flag output, does not terminate. When the flag is set to a one state, signifying the ending of the counting interval, the program then initiates an IOT 6142 pulse (D) which reads in the data. The program sequence to accomplish this is:

```
6141        /SKIP NEXT STEP IF FLAG = 1
JMP .-1     /JUMP BACK TO PREVIOUS STEP
6142        /READ IN DATA
```

Figure A2

Interface logic diagram.

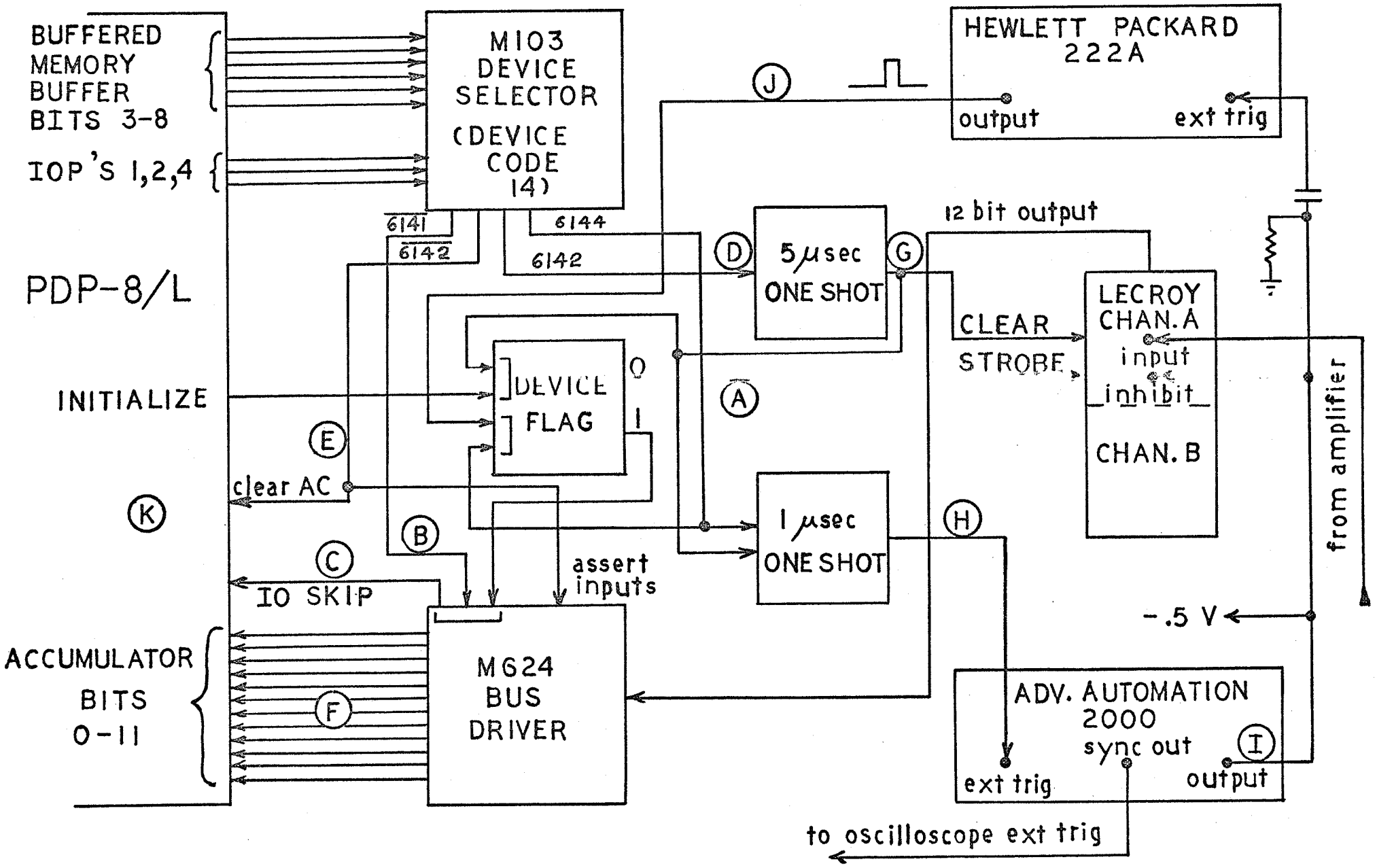
BUFFERED MEMORY BUFFER BITS 3-8
IOP'S 1,2,4
M103 DEVICE SELECTOR (DEVICE CODE 14)
6141
6142
6144
6142
PDP-8/L
INITIALIZE
DEVICE FLAG
0
1
clear AC
IO SKIP
assert inputs
ACCUMULATOR BITS 0-11
M624 BUS DRIVER
5 μsec ONE SHOT
1 μsec ONE SHOT
HEWLETT PACKARD 222A
output
ext trig
12 bit output
CLEAR
STROBE
LECROY CHAN. A
input
inhibit
CHAN. B
from amplifier
-.5 V
ADV. AUTOMATION 2000
sync out
ext trig
output
to oscilloscope ext trig
A
B
C
D
E
F
G
H
I
J
K

Figure A3

Interface timing diagram.

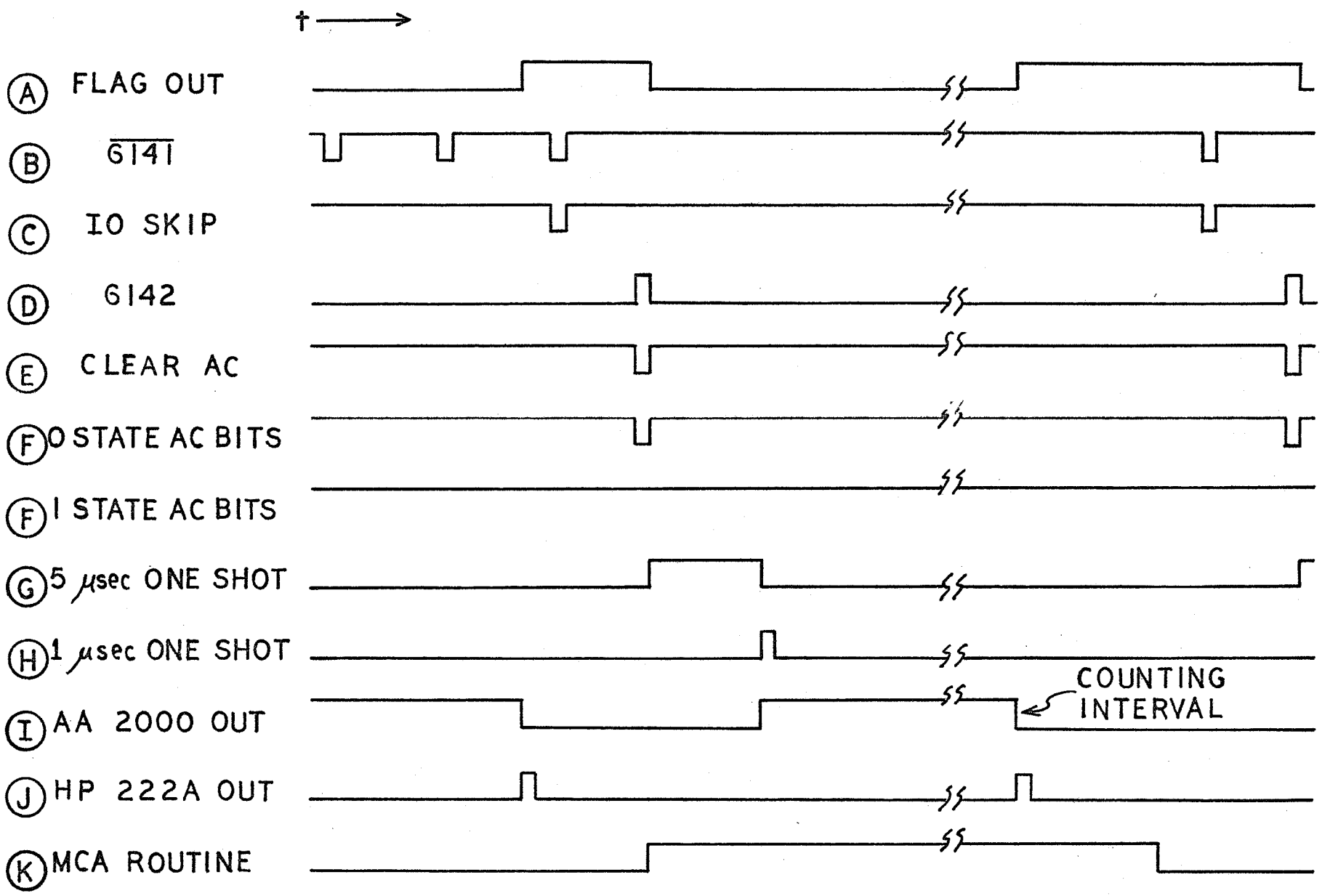
t
A FLAG OUT
B $\overline{6141}$
C IO SKIP
D 6142
E CLEAR AC
F 0 STATE AC BITS
F 1 STATE AC BITS
G 5 μsec ONE SHOT
H 1 μsec ONE SHOT
I AA 2000 OUT
COUNTING INTERVAL
J HP 222A OUT
K MCA ROUTINE

The 6142 pulse reads in the data in the following way:

1. The appearance of the flag also places the outputs of the first 12 bits of channel A of the Lecroy scaler on the inputs of the M624 bus driver. It does this by putting + 3 volts on the "strobe channel A" input of the scaler.
2. For the duration of the 6142 pulse, the outputs of the M624 bus driver and the clear AC are asserted. This accomplishes the loading of the data from the Lecroy into the PDP-8/L accumulator. Because of signal inversions, the complement of the data is actually read into the computer as in (F).

The trailing edge of DT 6142 triggers a one shot of 5 microseconds duration (G) which sumultaneously clears the Lecroy scaler and resets the device flag. The trailing edge of this one shot triggers another one shot of 1 microsecond duration (H), the output of which is used to trigger the AA 2000 generator (I), which times the counting interval, beginning the whole sequence again.

The length of the counting interval is set by the pulse width control of the AA generator. If it is necessary to separate counting intervals widely to insure counting of independent samples, the pulse delay control of the AA generator does the job.

The output of the AA generator is sent to the external trigger input of the HP 22A generator through a differentiator. The HP generator is set to trigger on the trailing edge of the AA timing pulse. The pulse from the HP generator is used to set the device flag, thus signaling the availability of data for the computer.

The timing diagram shows two sequences that can happen as far as the routine which waits for data is concerned. If the MCA routine is accomplished before the end of the counting interval, the IOT $\overline{6141}$ sequence of pulses will occur, waiting for a flag. If the MCA routine takes longer than the counting interval, the flag will be set and the first IOT $\overline{6141}$ will initiate read in of the data.

The IOT 6144 serves no function as far as routine read in of data is concerned. It can be used to set the device flag and trigger the 1 microsecond one shot

to provide test pulses to check the Lecroy scaler and the interface through the use of the PTEST program.

PTEST is a diagnostic program which checks out a portion of the interface and the operation of the Lecroy scaler, at least at relatively low frequencies, through the use of counting pulses generated in the interface. The next page gives a program listing of PTEST as well as instructions for its use.

6. The PTEST Program

```
                    /PTEST - DIAGNOSTIC PROGRAM
*5400
6144
6142
CMA
DCA STORØ           /TO RUN, PUT START COUNT INTO
TAD TWO1            /EXTERNAL TRIGGER INPUT OF
JMS COUNT           /HEWLETT PACKARD 222A GENERATOR
DCA STOR1           /REP. RATE -MAN./EXT. +
TAD TWO2            /PULSE DELAY - .5 USEC.
JMS COUNT           /PULSE WIDTH - .5 USEC
DCA STOR2           /PULSE POLARITY - NEGATIVE
TAD TWO3            /PULSE AMPLITUDE - .5 TO 1 VOLT
JMS COUNT           /OUTPUT TO LECROY CHANNEL A INPUT
DCA STOR3           /CHANNEL A ATTENUATOR - X5
TAD TWO4            /MANUAL BUTTON ON 222A SHOULD FLIP LECROY
JMS COUNT           /MAKE SURE INHIBIT ON LECROY IS OFF
DCA STOR4           /SET SWITCH REGISTER TO 7777
TAD TWO5            /LOAD PTEST USING BIN LOADER
JMS COUNT           /CLEAR LECROY CHANNEL A USING CLEAR
DCA STOR5           /BUTTON ON FRONT PANEL
TAD TWO6            /LOAD ADDRESS 54ØØ AND START PROGRAM
JMS COUNT           /PROGRAM HALTS AT 5445 WITHIN 1 SECOND
DCA STOR7           /CORRESPONDENCE SHOULD BE:
TAD TWO8            /ADDRESS          1 BIT (ALL OTHERS Ø)
JMS COUNT
DCA STOR8           /55ØØ                   11
TAD TWO9            /55Ø1                   1Ø
JMS COUNT           /55Ø2                   Ø9
DCA STOR9           /55Ø3                   Ø8
TAD TWO1Ø           /55Ø4                   Ø7
JMS COUNT           /55Ø5                   Ø6
DCA STOR1Ø          /55Ø6                   Ø5
TAD TWO11           /55Ø7                   Ø4
JMS COUNT           /551Ø                   Ø3
DCA STOR11          /5511                   Ø2
HLT                 /5512                   Ø1
COUNT, Ø            /5513                   ØØ
DCA STOP
6144
ISZ STOP
JMP .-2
6142
CMA
JMP I COUNT
STOP, Ø
```

```
TWO1, 7777
TWO2, 7775
TWO3, 7771
TWO4, 7761
TWO5, 7741
TWO6, 77Ø1
TWO7, 76Ø1
TWO8, 74Ø1
TWO9, 7ØØ1
TWO1Ø, 6ØØ1
TWO11, 4ØØ1

*55ØØ
STORØ, Ø
STOR1, Ø
STOR2, Ø
STOR3, Ø
STOR4, Ø
STOR5, Ø
STOR6, Ø
STOR7, Ø
STOR8, Ø
STOR9, Ø
STOR1Ø, Ø
STOR11, Ø
```

Figure A4

PDP-8/L photocount interface schematic.

Notes:

1. Connector designations:
   LCI - Interface input from Lecroy scaler
   LCO - Output connector on Lecroy scaler
   D34, D35, D36 designate both an output from the interface and an input to the computer, connected by ribbon cables.
2. All signal outputs of the Lecroy scaler are tied to ground through 1 KΩ at the scaler.
3. Supply voltages:
   +5VDC, PIN A2 of M112, M103, M624, M32
   GND - PINS T1 and C2, All connectors and modules
4. All gates marked g are on M112 module
5. + and - 6S are sensing leads to regulate the + and - 6V supply which supplies voltages to the Lecroy scaler.

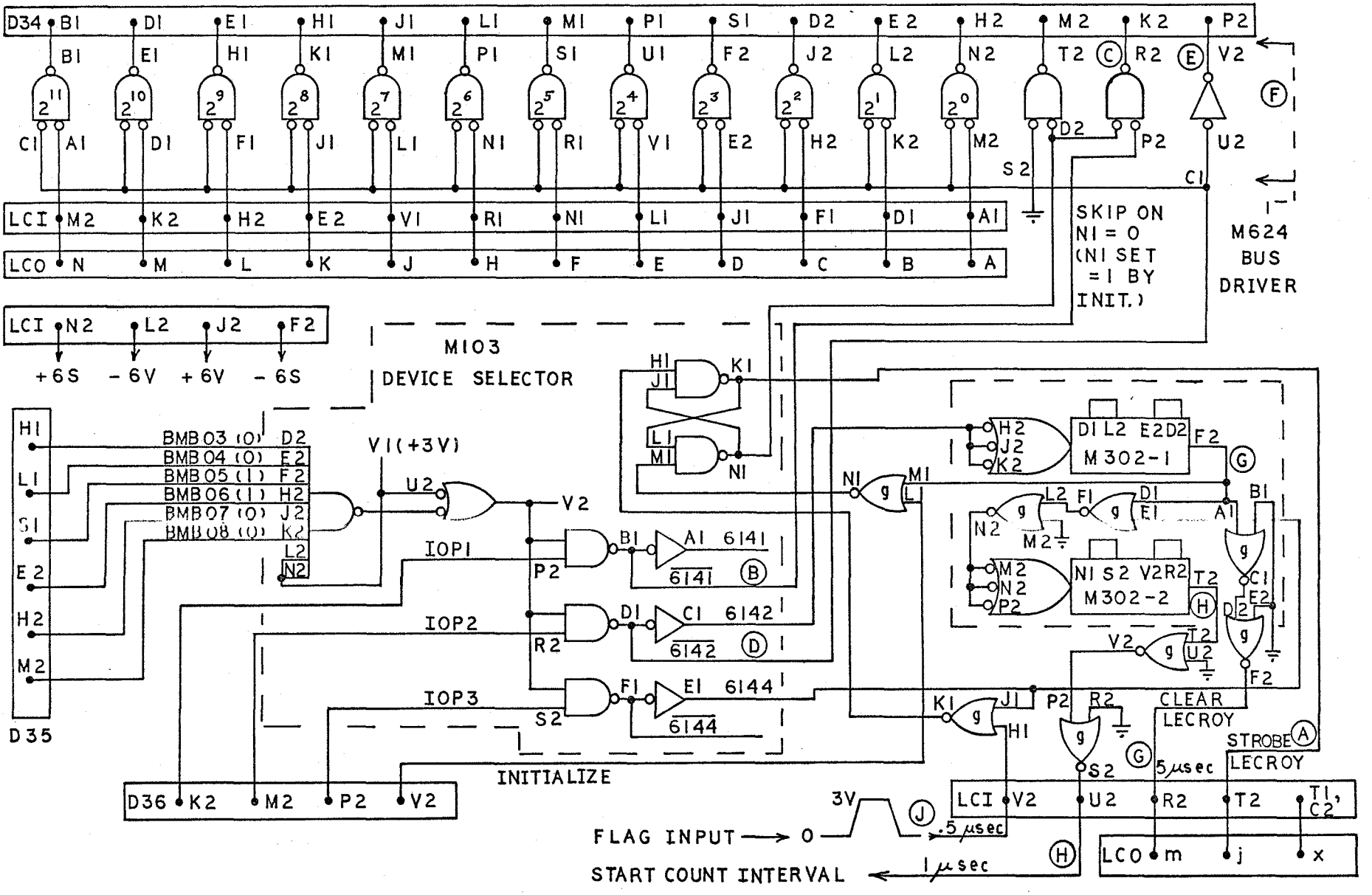
D34 B1 D1 E1 H1 J1 L1 M1 P1 S1 D2 E2 H2 M2 K2 P2
LCI M2 K2 H2 E2 V1 R1 N1 L1 J1 F1 D1 A1
LCO N M L K J H F E D C B A
SKIP ON NI = 0 (NI SET = 1 BY INIT.)
M624 BUS DRIVER
LCI N2 L2 J2 F2
+6S -6V +6V -6S
M103 DEVICE SELECTOR
BMB03 (0) D2
BMB04 (0) F2
BMB05 (1) F2
BMB06 (1) H2
BMB07 (0) J2
BMB08 (0) K2
V1 (+3V)
IOP1
IOP2
IOP3
INITIALIZE
D35
D36 K2 M2 P2 V2
6141
6142
6144
M302-1
M302-2
CLEAR LECROY
STROBE LECROY
5 μsec
3V
.5 μsec
1 μsec
FLAG INPUT
START COUNT INTERVAL
LCI V2 U2 R2 T2 T1, C2
LCO m j x

APPENDIX B

LOG-NORMAL DISTRIBUTION

Inputs: <N>, H2 and Number of Events, C

C-FOCAL,1969

```
Ø1.2Ø A ?NBAR?;T !;A ?H2?;T !;A ?C?
Ø1.3Ø S S2=(1/4)*FLOG(H2+1);S IØ=NB*FEXP(-2*S2)
Ø1.4Ø S N=Ø;S PS=Ø;S X=1;T !!!;S M=1; S SU=Ø
Ø1.41 D 5.Ø
Ø1.42 S MY=(IØ/3Ø)*4*Y;S PS=PS+MY
Ø1.44 I (MY-1.E-7)3.Ø1,3.Ø1,1.45
Ø1.45 S M=M+1;D 5.Ø
Ø1.46 S MY=(IØ/3Ø)*2*Y;S PS=PS+MY
Ø1.48 I (MY-1.E-7)3.Ø1,3.Ø1,1.49
Ø1.49 S M=M+1;GOTO 1.41

Ø2.1Ø S A=.933Ø78E-1;S H=.21[illegible]235EØ;D 4.Ø
Ø2.12 S A=.492692EØ;S H=.342[illegible]1ØEØ;D 4.Ø
Ø2.14 S A=.12156ØE1;S H=.263[illegible]28EØ;D 4.Ø
Ø2.16 S A=.226995E1;S H=.126[illegible]26EØ;D 4.Ø
Ø2.18 S A=.366762E1;S H=.4Ø2[illegible]69E-1;D 4.Ø
Ø2.2Ø S A=.542534E1;S H=.856[illegible]38E-2;D 4.Ø
Ø2.22 S A=.756592E1;S H=.121[illegible]44E-2;D 4.Ø
Ø2.24 S A=.1Ø12Ø2E2;S H=.111[illegible]74E-3;D 4.Ø
Ø2.26 S A=.1313Ø3E2;S H=.645[illegible]93E-5;D 4.Ø
Ø2.28 S A=.166544E2;S H=.222[illegible]32E-6;D 4.Ø
Ø2.3Ø S A=.2Ø7765E2;S H=.422[illegible]43E-8;D 4.Ø
Ø2.32 S A=.256239E2;S H=.392[illegible]39E-1Ø;D 4.Ø
Ø2.34 S A=.314Ø75E2;S H=.145[illegible]52E-12;D 4.Ø
Ø2.36 S A=.3853Ø7E2;S H=.148[illegible]Ø3E-15;D 4.Ø
Ø2.38 S A=.48Ø261E2;S H=.162[illegible]6ØE-19;D 4.Ø
Ø2.40 GOTO 3.Ø1
```

```
Ø3.Ø1 S P=PS/(2*X*FSQT(6.283?9*S2))
Ø3.1Ø T %3.Ø,"P(",?N?,")",%,P,"      ",FSQT(P/C),!
Ø3.2Ø S N=N+1;S X=N*X;S PS=P
Ø3.21 S SU=SU+P
Ø3.3Ø I (P-1.ØE-7)3.95,3.95,3.1Ø
Ø3.95 T %,!,?SUM?,!!
Ø3.96 Q

Ø4.Ø4 S PS=PS+H*A↑(N-1)*FEXP(-(FLOG(A/IØ))↑2/(8*S2))
Ø4.05 R

Ø5.Ø1 S Y=(1Ø/(M*IØ))*FEXP(-(M*IØ/1Ø-(FLOG(M/1Ø))↑2/(8*S2))
*
```

APPENDIX C

COMPARISON OF GAUSS-LAGUERRE INTEGRATION AND NUMERICAL INTEGRATION

LOG NORMAL DISTRIBUTION

NBAR:1.Ø714655

H2:.3157846

		NUMINT
P(N= Ø)=	Ø.392495E+ØØ	.3923933
P(N= 1)=	Ø.3241Ø9E+ØØ	.3259551
P(N= 2)=	Ø.165652E+ØØ	.1678545
P(N= 3)=	Ø.7Ø5223E-Ø1)	.0707399
P(N= 4)=	Ø.272267E-Ø1	.0271630
P(N= 5)=	Ø.1ØØ417E-Ø1	.0100293
P(N= 6)=	Ø.366866E-Ø2	.0036697
P(N= 7)=	Ø.135391E-Ø2	.0013543
P(N= 8)=	Ø.5Ø9423E-Ø3	.0005094
P(N= 9)=	Ø.196486E-Ø3	.0001965
P(N= 1Ø)=	Ø.779558E-Ø4	.0000780
P(N= 11)=	Ø.318665E-Ø4	.0000319
P(N= 12)=	Ø.134253E-Ø4	.0000134
P(N= 13)=	Ø.582694E-Ø5	.0000058
P(N= 14)=	Ø.26Ø332E-Ø5	.0000026
P(N= 15)=	Ø.119596E-Ø5	.0000012
P(N= 16)=	Ø.564242E-Ø6	.0000006
P(N= 17)=	Ø.273Ø35E-Ø6	
P(N= 18)=	Ø.135334E-Ø6	
P(N= 19)=	Ø.686236E-Ø7	

SUM= Ø.9959Ø7E+ØØ

*

REFERENCES

1. See, for example, A. Sommerfeld, Optics (Academic, New York, 1954) p. 196.

2. W. Martienssen and E. Spiller, Am. J. Phys. 32, 919 (1964); F. T. Arecchi, Phys. Rev. Letters 15 912 (1965).

3. F. T. Arecchi, M. Giglio and U. Tartari, Phys. Rev. 163, 186 (1967); N. A. Clark, J. H. Lunacek, and G. B. Benedek, Am. J. Phys. 38, 575 (1970).

4. F. T. Arecchi, in Quantum Optics, edited by R. J. Glauber (Academic, New York, 1970) p. 101.

5. Two authoritative reviews on the problem of light scattering from thermodynamical fluctuations are: I. L. Fabelinskii, Molecular Scattering of Light (Plenum, New York, 1968) and G. B. Benedek, in Ninth Brandeis Summer Institute in Theoretical Physics (Gordon and Breach, New York, 1968).

6. Approximate specification from the Spectra-Physics Model 119 laser Instruction Manual.

7. J. W. Goodman, Introduction to Fourier Optics (McGraw-Hill, New York, 1968) p. 60.

8. R. P. Feynman and A. R. Hibbs, Quantum Mechanics and Path Integrals (McGraw-Hill, New York, 1965) p. 357.

9. V. V. Anisimov, S. M. Kozel, and G. R. Lokshin, Opt. Specktrosk. 27, 258 (1969).

10. Ref. 4., p. 100.

11. See, for example, M. J. Lighthill, Introduction to Fourier Analysis and Generalised Functions (University Press, Cambridge, 1958) p. 29 and E. Guillemin, Theory of Linear Physical Systems (Wiley, New York, 1963) p. 348.

12. F. Reif, Fundamentals of Statistical and Thermal Physics (McGraw-Hill, New York, 1965) p. 585.

13. See G. B. Benedek, reference 5, pp. 92-98.

14. C. Freed and H. Haus, Phys. Rev. 141, 287 (1966).

15. M. C. Wang and G. Uhlenbeck, Rev. Mod. Phys. 17, 326 (1945).

16. N. C. Ford and G. B. Benedek, Phys. Rev. Letters 15, 649 (1965).

17. An extensive bibliography of photon counting literature appears in J. D. Kuppenheimer Jr., "Intensity and Phase Modulation of Laser Beams and Photon Count Distributions" (unpublished Ph.D. dissertation, Worcester Polytechnic Institute, 1969).

18. L. Mandel, in Progress in Optics, Vol. 2, edited by E. Wolf (North-Holland, Amsterdam, 1963). Also L. Mandel and E. Wolf, Rev. Mod. Phys. 37, 231 (1965).

19. W. G. Clark, "Photoelectron Counting Distributions of Modulated and Second Harmonic Generated Light Beams" (unpublished Ph.D. dissertation, Worcester Polytechnic Institute, 1971).

20. J. W. Strutt (Lord Rayleigh), The Theory of Sound (Dover, New York, 1945) pp. 35-42.

21. R. J. Glauber, Phys. Rev. 131, 2766 (1963)

22. E. Butkov, Mathematical Physics (Addison Wesley, Reading, Mass., 1968) p. 299.

23. Reference 17, p. 54.

24. Reference 4, p. 68.

25. H. Cramer, Mathematical Methods of Statistics (Princeton University Press, Princeton, 1946) p. 186.

26. Ibid. p. 188.

27. Reference 17, p. 57.

28. See Reference 17.

29. Reference 4, p. 74. Also Reference 31, p. 66.

30. V. I. Tatarski, Wave Propagation in a Turbulent Medium (McGraw-Hill, New York, 1961); L. A. Chernov, Wave Propagation in a Random Medium (McGraw-Hill, New York, 1960); J.W. Strohbehn, Proc. IEEE 56, 1301 (1968).

31. G. F. Riley, "Experimental Determination of the Probability Distribution for Irradiance Fluctuations of Laser Beams in a Turbulent Atmosphere by Photon Counting" (unpublished Ph.D. dissertation, Worcester Polytechnic Institute, 1970).

32. See reference 19, Appendix A.

33. Reference 8.

34. P. Diament and M. C. Teich, JOSA 60, 1489 (1970).

35. Reference 31, p. 49.

36. G. Arfken, Mathematical Methods for Physicists (Academic, New York, 1970) p. 373.

37. Private communication with Dr. Riley.

38. Z. Kopal, Numerical Analysis (Chapman and Hall, London, 1955). The coefficients for the Gauss-Laguerre integration are on p. 371. The Simpsons rule integration is on p. 406.

39. Ibid., p. 525. See also M. Abramowitz and I. A. Stegun, Handbook of Mathematical Functions (U. S. Government Printing Office, Washington, D. C., 1964) p. 923.

40. Mr. Ernie Gustafson of the Norton Company kindly furnished several abrasive samples.

41. L. R. Wilcox, IEEE Journal of Quantum Electronics 2, 557 (1966).

42. L. E. Estes, L. M. Narducci, and R. A. Tuft, to be published in JOSA 61. (1971). The article will probably appear in the September issue.

PART II. Photoelectron Counting Distribution of Second Harmonic Light Generated by a Pseudo-thermal Source(*)

William G. Clark, Lee E. Estes, and Lorenzo M. Narducci

Worcester Polytechnic Institute

Worcester, Massachusetts 01609

Abstract

We calculate the photoelectron counting distribution for second-harmonic light generated by a monochromatic, single-mode, thermal light source and compare our predictions with experimental results using as a fundamental light source a suitably modulated laser beam.

(*) This work was partially supported by NASA Grant NGR 22-017-019 (1970-71) and NSF Initiation Grant GK-5517.

Introduction

The purpose of the present communication is that of presenting a few theoretical and experimental results concerning the photoelectron statistics of the second harmonic radiation produced by a light beam whose irradiance fluctuations are those of a thermal source.

Because of the nonlinear nature of the second-harmonic generation (S.H G.) process, irradiance fluctuations that are present in the fundamental beam are expected to produce quite different fluctuations in the second harmonic radiation.

A well-known source exhibiting irradiance fluctuations is a light beam with a gaussian field amplitude probability density and zero mean. Although such a source can be conveniently prepared by suitably modulating a stable He-Ne laser beam by means of a rotating ground glass with small average inhomogeneities[1], our presently available power levels are not high enough to produce detectable second-harmonic signals.

In the present investigation we have electronically modulated the output of a He-Ne laser in such a way that the irradiance fluctuations are very close to those of a narrow band, polarized thermal beam. The photoelectron distribution derived in the theoretical section of this paper has been favorably compared with the experimentally measured distributions.

Theoretical outline

When a beam of light is incident on a photomultiplier for a time interval T the resulting distribution of photoelectrons can be predicted by averaging the Poisson process of photoemission over the possible realizations of the field irradiance $I(t)$. If the measurements are made within a coherence volume of the light, the probability $P(n)$ that n photoelectrons

are ejected in the time interval T is given by[2]

$$p(n) = \left\langle \frac{(\beta I T)^n}{n!} \exp(-\beta I T) \right\rangle_I \qquad (1)$$

where β is a constant which accounts for the geometry of the experiment and the quantum efficiency of the photosensitive surface. The brackets, $\langle\ \rangle$, indicate that an ensemble average is taken over the irradiance fluctuations. For the low irradiance levels used in our experiments the process of S.H.G. can be accurately described by the expression[3]

$$I_{SH} = \kappa I_F^2 \qquad (2)$$

which relates the irradiance I_{SH} of the second harmonic to the irradiance I_F of the fundamental beam. The constant κ is determined by the degree of phase matching and the magnitude of the nonlinear polarizability. Combining eq's. (1) and (2), one obtains the counting distribution for the second harmonic radiation,

$$p(n) = \left\langle \frac{(\beta \kappa T I_F^2)^n}{n!} \exp(-\beta \kappa T I_F^2) \right\rangle_{I_F} . \qquad (3)$$

We shall perform the average indicated in eq. (3) for two special cases. In the first case we consider a fundamental light beam which is generated by a single mode amplitude-stabilized laser. If the irradiance of the laser beam is I_L, the irradiance probability distribution of the fundamental beam is a delta function $\delta(I_F - I_L)$, and eq. (3) yields a Poisson distribution of photoelectrons,

$$p(n) = \frac{(\beta \kappa T I_L^2)^n}{n!} \exp(-\beta \kappa T I_L^2) . \qquad (4)$$

Experiments have been performed to test eq. (4) and the results which have appeared in an earlier publication[4] are in good agreement with this result.

The second case considered here is that of a single mode laser beam which is modulated to produce irradiance fluctuations that are described by the probability distribution $P(I_F)$,

$$P(I_F) = \frac{1}{\langle I_F \rangle} \exp\left(-\frac{I_F}{\langle I_F \rangle}\right) . \tag{5}$$

This distribution function is characteristic of a single mode narrow band thermal beam and the combination of eq's. (1) and (5) yields the familiar Bose-Einstein distribution of photoelectrons,

$$p(n) = \frac{\left(\beta \tau \langle I_F \rangle\right)^n}{\left(1 + \beta \tau \langle I_F \rangle\right)^{n+1}} . \tag{6}$$

While the lack of irradiance fluctuations in the first case produced a Poisson distribution for both the fundamental and the second-harmonic beams, in this case we can expect the nonlinear process of second-harmonic generation to enhance the fluctuations of the fundamental beam, thus producing photoelectron statistics that no longer follow the Bose-Einstein distribution.

Using eq. (5), eq. (3) takes the form

$$p(n) = \int_0^\infty dI_F \, \frac{\left(\beta \kappa \tau I_F^2\right)^n}{n!} \exp\left(-\beta \kappa \tau I_F^2\right) \times \tag{7}$$

$$\times \frac{1}{\langle I_F \rangle} \exp\left(-\frac{I_F}{\langle I_F \rangle}\right) .$$

The result of the integration is the photoelectron distribution

$$p(n) = a(2n-1)!! \exp\left(\frac{a^2}{4}\right) D_{-(2n+1)}(a) \qquad (8)$$

where $a = \left(\chi\beta T \langle I_F \rangle\right)^{-1/2}$ and $D_{-(2n+1)}(a)$ is the parabolic cylinder function.[5] As expected, the two beams produce quite different photoelectron statistics.

Experimental Results

The preparation of a pseudo-thermal source (i.e., a source exhibiting the irradiance fluctuations that are typical of narrow-band blackbody radiation) to be used as the fundamental beam in the S.H.G. experiment presents two main difficulties. First of all, the low power level (7 mW) of the single-mode He-Ne Spectra Physics Model 120 laser does not allow the sizable power loss which would arise from conventional random modulation (e.g. rotating ground glass). Secondly, the index-matching condition requires that the angle of incidence of the fundamental beam on the ADP crystal remain fixed throughout the duration of the experiment.

We chose to pass the laser beam through a Pockel cell modulator exhibiting an extinction ratio of 500:1 as shown in fig. 1. The modulating voltage to be applied to the Pockel cell was produced by a signal recorded on magnetic tape and amplified by a 1000 gain 2500 volt power amplifier with a linear frequency response from 10 Hz to 15 kHz. The time-dependent behavior of this signal, which was originally produced by a Hybrid computer, was such that the probability distribution $P(I_F)$ of the modulated irradiance would closely approximate eq. 5.

Experiments performed on the modulated laser beam resulted in the photoelectron counting distribution shown in fig. 2. It will be noted that the largest deviation from the theoretical Bose-Einstein distribution

occurs for low values of the photoelectron number n. This we attribute to some low-frequency distortion in the modulating voltage, caused by the amplifier. Since at low irradiance levels, the amount of second-harmonic radiation is also low, it is expected that a somewhat better agreement will exist between the experimental and the theoretical photoelectron counting distributions generated by the second harmonic radiation.

A typical experimental distribution of photoelectrons is shown in fig. 3 together with the theoretical prediction and with a Bose-Einstein distribution corresponding to the experimental mean number of photoelectrons.

Although a small systematic deviation exists between the experimental and theoretical results we find the overall agreement quite satisfactory.

Acknowledgments

We wish to acknowledge the kindness of Itek Corporation and the American Optical Corporation respectively for the loan of the Pockel cell unit and of the ADP crystal. We are also grateful to Dr. J Kuppenheimer for useful suggestions and comments.

REFERENCES

1. L. E. Estes, L. M. Narducci, R A. Tuft, "The Scattering of Light from a Rotating Ground Glass," JOSA (to be published).

2. L. Mandel, E. Wolf, Rev. Mod. Phys. 37, 231, (1965).

3. J. Ducuing, N. Bloemberger, Phys. Rev. 133, 1493 (1964).

4. W. G. Clark, L. E. Estes, L. M Narducci, Phys. Lett. 33A, 517, (1970).

5. M. Abramowitz, I. Stegun, Handbook of Mathematical Functions, Dover, N.Y., pg 687 eq. 19.3.7.

FIGURE CAPTIONS

Figure 1. Schematic diagram of the experiment.
(1) laser; (2) 6328Å interference filter; (3) tape deck;
(4) 2500 volt amplifier; (5) Pockel cell; (6) ADP crystal;
(7) Shott UG-5 filters; (8) 3164Å interference filter;
(9) Amperex XP-1021 photomultiplier; (10) to counting system

Figure 2. Photoelectron counting statistics of the pseudo-thermal source. Mean number of counts $\bar{n}$ = 1.93 and the integration time = 50 μs. Curve No. 1 is the theoretical Bose-Einstein distribution and curve No. 2 is the experimental counting distribution obtained by modulating the laser beam.

Figure 3. Photoelectron counting statistics of the second harmonic light generated by the pseudo-thermal source. The mean number of counts is $\bar{n}$ = 2.84 and the integration time T = 50 μs. Curve No. 1 is the theoretical distribution and curve No. 2 represents the experimental results. Curve No. 3 is the Bose-Einstein distribution for the same mean number.

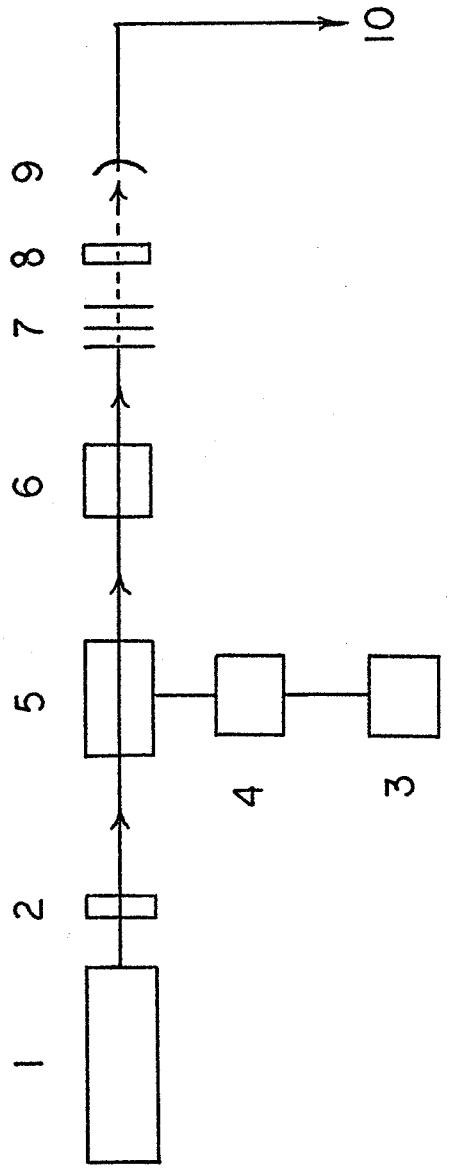
1
2
3
4
5
6
7
8
9
10

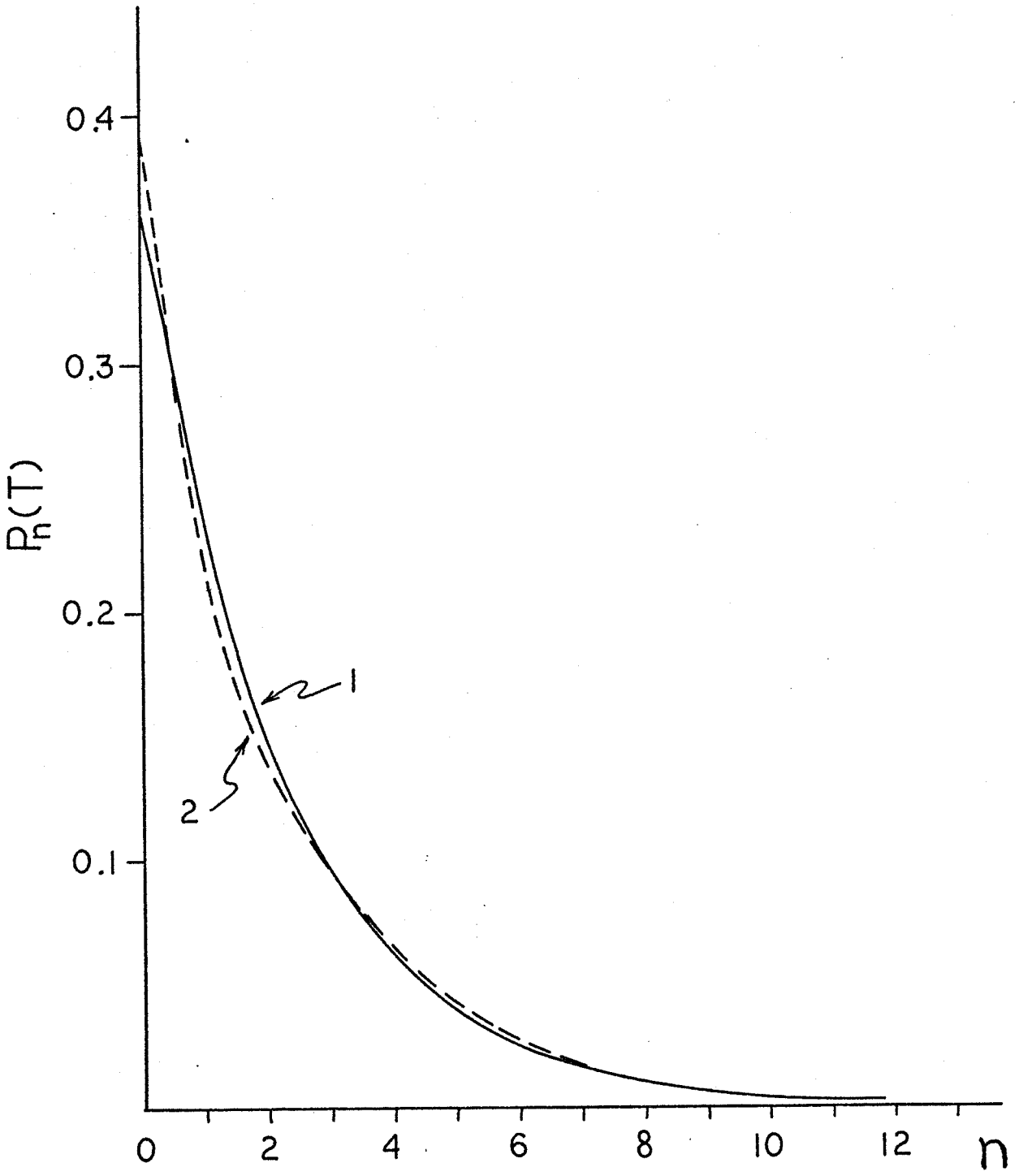

Clark et al fig 2

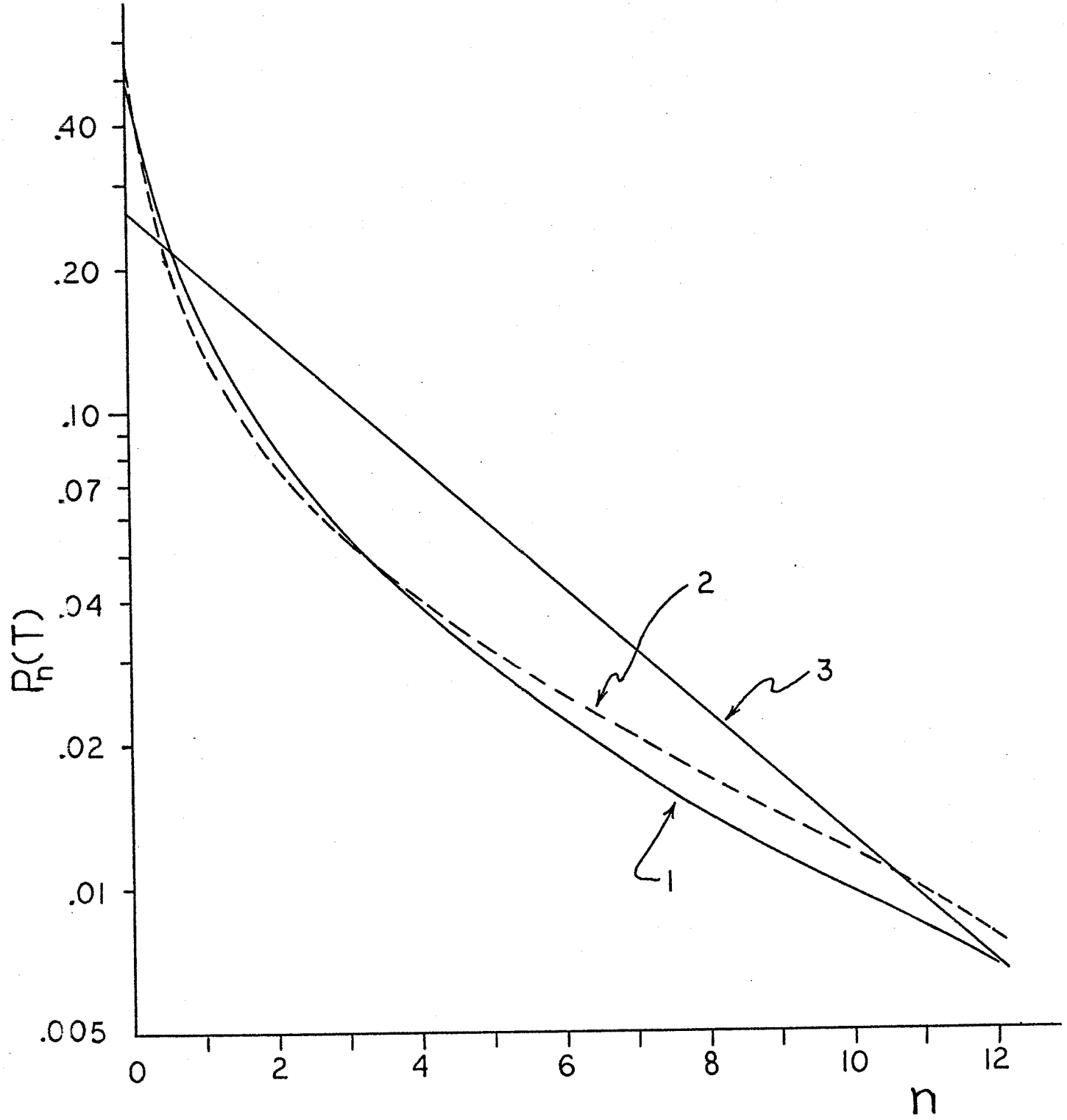
.40
.20
.10
.07
.04
.02
.01
.005
$P_n(T)$
0
2
4
6
8
10
12
n
1
2
3

PART III A BRIEF NOTE ON THE UPPER BOUND OF THE OPTICAL TRANSFER FUNCTION (OTF).

For two decades now, workers in optics have been applying the methods of electrical communication theory to optical systems treated as filters of spatial frequencies. While the success of this approach is based upon the similarity of the two fields (linear filter theory), it is important to recognize that there are essential differences. For example, in electric circuit theory, the impulse response h(t) is necessarily causal [$h(t)=0,\ t<0$]. This condition imposes severe restrictions on the physical realizability of the electrical frequency response $H(\omega)$; the real and imaginary parts of which are constrained to be Hilbert transform pairs.

In optics, the impulse response s(x), being the intensity of light in the point image, is necessarily a non-negative function. An interesting question that arises there is whether or not this restriction imposes unique conditions on the optical transfer function $\mathcal{T}(\omega)$. So far as we can ascertain, this is still an unsolved mathematical problem. Nevertheless, the non-negativeness of s(x) does impose an upper bound on $\mathcal{T}(\omega)$. The solution to this problem in fact, has existed in the optical literature for some time. Lukosz[1] in 1962 provided the answer in one dimension and more recently (1969) Frieden[2] gave the two-dimensional solution. In the course of our research, we discovered a simpler proof of the theorem using the Schwartz inequality and, in addition, determined the optimum lens coating to achieve the upper bound for each ω. Curves illustrating the upper bounds in one and two dimensions

are shown in Figures III. 1 and III. 2. The more important features of the analysis are listed as follows:

1) Midway toward the diffraction limit (ω=2), a uniform amplitude across the entire pupil is optimum. No amount of apodization (coating) or phase variations (aberrations) can achieve an OTF higher than $\tau_1 = 1/2$ at ω=1. In two dimensions the upper bound is $\tau_2 = .393$ at $\omega = 1$.

2) In the range $1 < \omega < 2$, a pair of slits represents the optimum coating While the slit width is different for each ω, an upper bound of $\tau = 1/2$ can be achieved anywhere in this band. The corresponding solution in two dimensions is an annular aperture.

3) In the range $0 < \omega < 1$, the optimum coating reduces to discontinuous rectangles which yield Lukosz's upper bound $\tau \leq \cos \frac{\pi}{N+1}$. In two dimensions, Frieden's upper bound is reached by sets of concentric circles properly weighted in transmission.

4) In the very low frequency regions $\omega << 2$, the asymptotic solution in one dimension reduces to a cosine tapering of the pupil with the first zero at the edge and in two dimensions the corresponding solution is a zero order Bessel function.

REFERENCES

Lukosz, W., Optica Acta, 9, 4, 335 (1962).

Frieden, B.R., JOSA, 59, 4, 402 (1969).

W. Lukosz (1962) - Optica Acta 9 4 p. 335

$\tau(\omega) \leq \cos \frac{\pi}{N+1}$

$\frac{\omega}{2} = \frac{1}{N}$

---- Conventional OTF

——— Upper bound

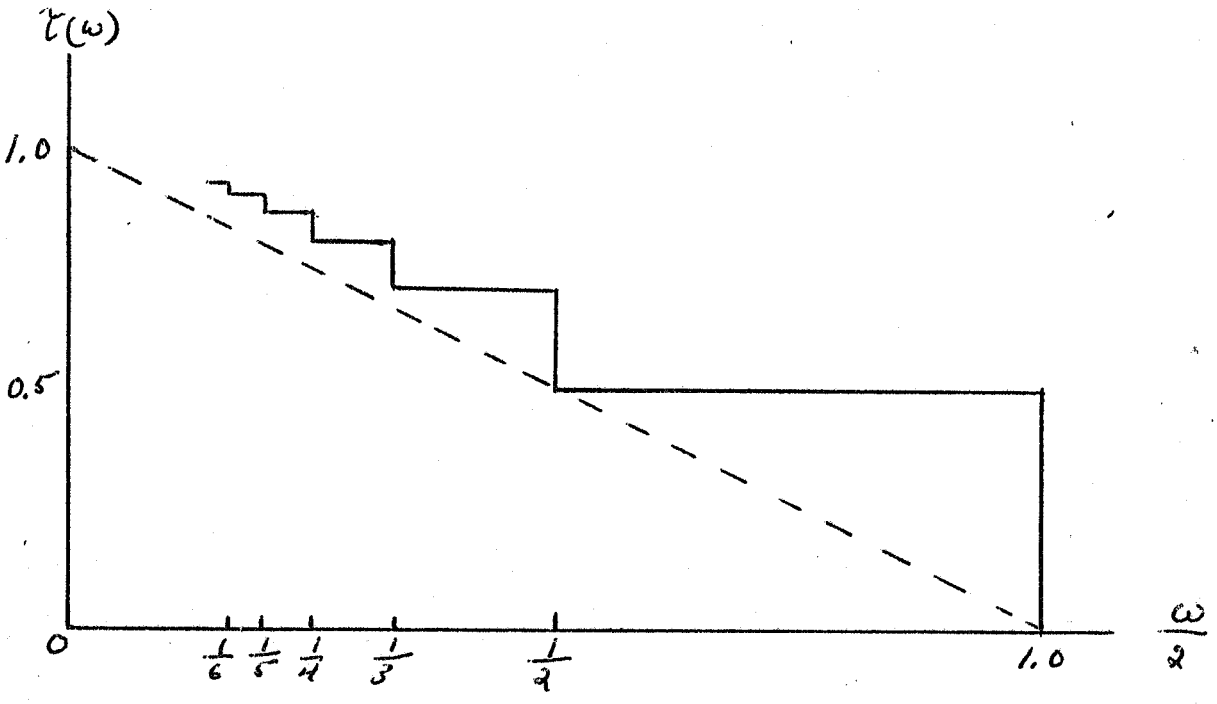

Fig III.1

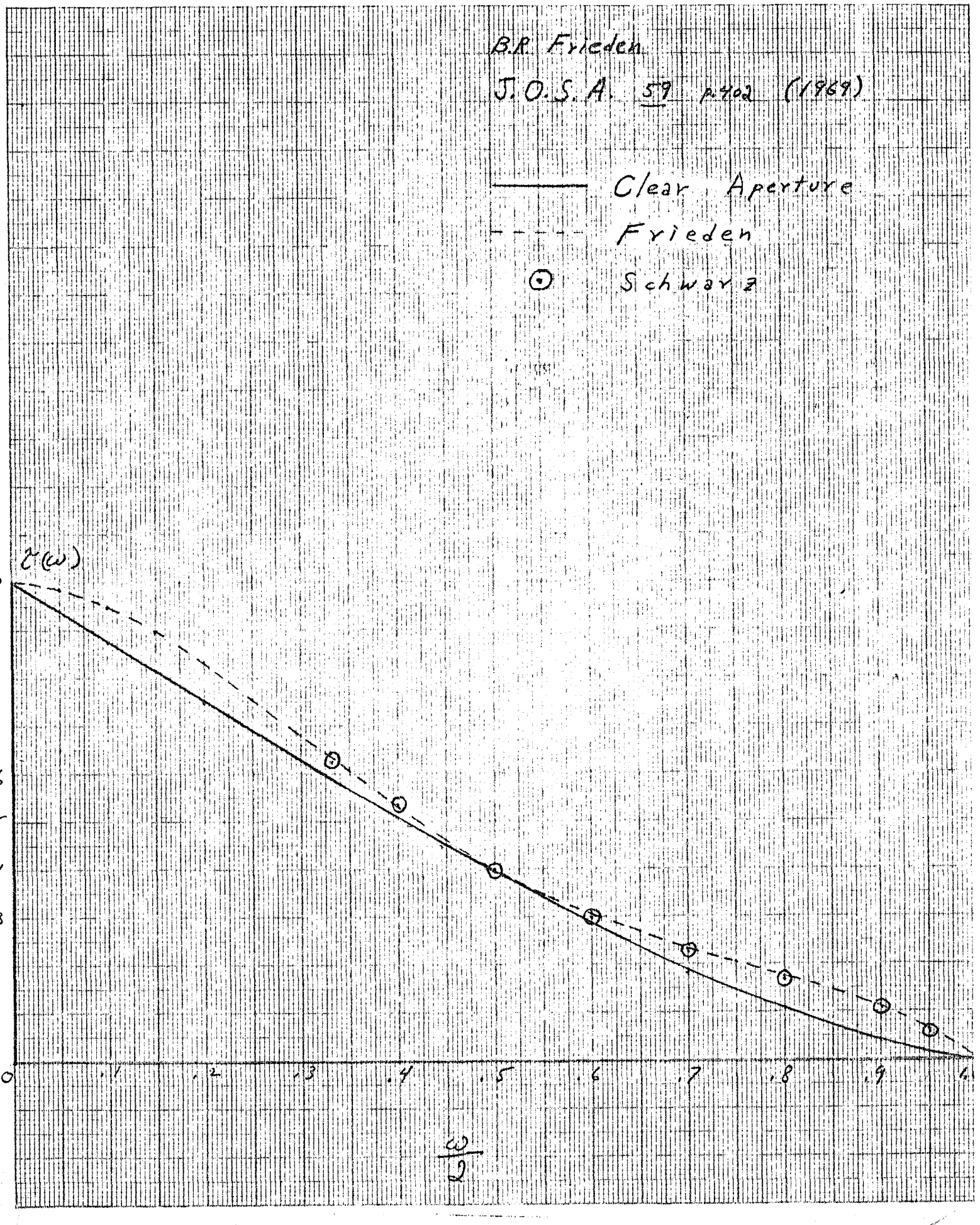
B.R. Frieden
J.O.S.A. 59 p.402 (1969)
Clear Aperture
Frieden
Schwarz
$\mathcal{L}(\omega)$
1.0
.9
.8
.7
.6
.5
.4
.3
.2
.1
0
.1
.2
.3
.4
.5
.6
.7
.8
.9
$\frac{\omega}{\Omega}$

Fig III-2